Theses and Dissertations   Thesis and Dissertation Collection

1994-03

Flight dynamics of an unmanned aerial vehicle

Watkiss, Eric John

Monterey, California. Naval Postgraduate School

http://hdl.handle.net/10945/28222

Flight Dynamics of an
Unmanned Aerial Vehicle

by

Eric John Watkiss
Lieutenant, United States Navy
Bachelor of Aerospace Engineering
Georgia Institute of Technology, 1986

Submitted in partial fulfillment of the
requirements for the degree of

MASTER OF SCIENCE IN AERONAUTICAL ENGINEERING

from the

NAVAL POSTGRADUATE SCHOOL
March 1994

REPORT DOCUMENTATION PAGE

Form Approved
OMB No. 0704-0188

1a. REPORT SECURITY CLASSIFICATION	1b. RESTRICTIVE MARKINGS
Unclassified	

2a. SECURITY CLASSIFICATION AUTHORITY	3. DISTRIBUTION/AVAILABILITY OF REPORT
2b. DECLASSIFICATION/DOWNGRADING SCHEDULE	Approved for public release; distribution is unlimited.

4. PERFORMING ORGANIZATION REPORT NUMBER(S)

5. MONITORING ORGANIZATION REPORT NUMBER(S)

6a. NAME OF PERFORMING ORGANIZATION	6b. OFFICE SYMBOL (If applicable)	7a. NAME OF MONITORING ORGANIZATION
Naval Postgraduate School	AA	Naval Postgraduate School

6c. ADDRESS (City, State, and ZIP Code)	7b. ADDRESS (City, State, and ZIP Code)
Monterey, CA 93943-5000	Monterey, CA 93943-5000

8a. NAME OF FUNDING/SPONSORING ORGANIZATION	8b. OFFICE SYMBOL (If applicable)	9. PROCUREMENT INSTRUMENT IDENTIFICATION NUMBER

8c. ADDRESS (City, State, and ZIP Code)	10. SOURCE OF FUNDING NUMBERS			
	PROGRAM ELEMENT NO.	PROJECT NO.	TASK NO.	WORK UNIT ACCESSION NO.

11. TITLE (Include Security Classification)
FLIGHT DYNAMICS OF AN UNMANNED AERIAL VEHICLE

12. PERSONAL AUTHOR(S)
Eric John Watkiss

13a. TYPE OF REPORT	13b. TIME COVERED	14. DATE OF REPORT (Year,Month,Day)	15. PAGE COUNT
Master's Thesis	FROM _____ TO _____	March 1994	94

16. SUPPLEMENTARY NOTATION
The views expressed in this thesis are those of the author and do not reflect the official policy or position of the Department of Defense or the U.S. Government.

17.	COSATI CODES		18. SUBJECT TERMS (Continue on reverse if necessary and identify by block number)
FIELD	GROUP	SUB-GROUP	Unmanned Aerial Vehicle, UAV, Flight Test, Flight Dynamics

19. ABSTRACT (Continue on reverse if necessary and identify by block number)

Moments of inertia were experimentally determined and longitudinal and lateral/directional static and dynamic stability and control derivatives were estimated for a fixed wing Unmanned Air Vehicle (UAV). Dynamic responses to various inputs were predicted based upon the estimated derivatives. A divergent spiral mode was revealed, but no particularly hazardous dynamics were predicted. The aircraft was then instrumented with an airspeed indicator, which when combined with the ability to determine elevator deflection through trim setting on the flight control transmitter, allowed for the determination of the aircraft's neutral point through flight test. The neutral point determined experimentally corresponded well to the theoretical neutral point. However, further flight testing with improved instrumentation is planned to raise the confidence level in the neutral point location. Further flight testing will also include dynamic studies in order to refine the estimated stability and control derivatives.

20. DISTRIBUTION/AVAILABILITY OF ABSTRACT	21. ABSTRACT SECURITY CLASSIFICATION
[X] UNCLASSIFIED/UNLIMITED ☐ SAME AS RPT. ☐ DTIC USERS	Unclassified

22a. NAME OF RESPONSIBLE INDIVIDUAL	22b. TELEPHONE (Include Area Code)	22c. OFFICE SYMBOL
Richard M. Howard	(408) 656 - 2870	AA/Ho

DD Form 1473, JUN 86   Previous editions are obsolete.   SECURITY CLASSIFICATION OF THIS PAGE

S/N 0102-LF-014-6603

Unclassified

ABSTRACT

Moments of inertia were experimentally determined and longitudinal and lateral/directional static and dynamic stability and control derivatives were estimated for a fixed wing Unmanned Air Vehicle (UAV). Dynamic responses to various inputs were predicted based upon the estimated derivatives. A divergent spiral mode was revealed, but no particularly hazardous dynamics were predicted. The aircraft was then instrumented with an airspeed indicator, which when combined with the ability to determine elevator deflection through trim setting on the flight control transmitter, allowed for the determination of the aircraft's neutral point through flight test. The neutral point determined experimentally corresponded well to the theoretical neutral point. However, further flight testing with improved instrumentation is planned to raise the confidence level in the neutral point location. Further flight testing will also include dynamic studies in order to refine the estimated stability and control derivatives.

TABLE OF CONTENTS

NOMENCLATURE

AAA	Anti-aircraft artillery
AoA	Angle of attack
AR	Wing aspect ratio
AR_t	Horizontal tail aspect aatio
AR_v	Vertical tail aspect ratio
b	Wing span
b_t	Horizontal tail span
b_v	Vertical tail height
c	Wing chord
c-bar, $\bar{c}$	Wing mean aerodynamic chord
C_D	Coefficient of drag
C_{D_0}	Coefficient of drag at zero lift

$$C_{D_\alpha} = \frac{\partial C_D}{\partial \alpha}$$

$$C_{D_q} = \frac{\partial C_D}{\partial \frac{q\bar{c}}{2V}}$$

$$C_{D_{\delta e}} = \frac{\partial C_D}{\partial \delta e}$$

C.G.	Center of gravity
C_L	Coefficient of lift
C_{L_t}	Coefficient of lift, tail

$$C_{L_{t_{\delta e}}} = \frac{\partial C_{L_t}}{\partial \delta e}$$

$$C_{L_\alpha} = \frac{\partial C_L}{\partial \alpha}$$

$$C_{L_{\dot{\alpha}}} = \frac{\partial C_L}{\partial \frac{\dot{\alpha}\bar{c}}{2V}}$$

$$C_{L_{\delta e}} = \frac{\partial C_L}{\partial \delta e}$$

$$C_{L_q} = \frac{\partial C_L}{\partial \frac{q\bar{c}}{2V}}$$

$C_{L_{trim}}$	Coefficient of lift in the trimmed condition

C_l Coefficient of rolling moment

$C_{l_p} = \dfrac{\partial C_l}{\partial \frac{pb}{2V}}$

$C_{l_r} = \dfrac{\partial C_l}{\partial \frac{rb}{2V}}$

$C_{l_\beta} = \dfrac{\partial C_l}{\partial \beta}$

$C_{l_{\delta a}} = \dfrac{\partial C_l}{\partial \delta a}$

$C_{l_{\delta r}} = \dfrac{\partial C_l}{\partial \delta r}$

C_m Coefficient of pitching moment

$C_{m_\alpha} = \dfrac{\partial C_m}{\partial \alpha}$

$C_{m_{\dot{\alpha}}} = \dfrac{\partial C_m}{\partial \frac{\dot{\alpha}\bar{c}}{2V}}$

$C_{m_{\delta e}} = \dfrac{\partial C_m}{\partial \delta e}$

$C_{m_q} = \dfrac{\partial C_m}{\partial \frac{q\bar{c}}{2V}}$

C_n Coefficient of yawing moment

$C_{n_p} = \dfrac{\partial C_n}{\partial \frac{pb}{2V}}$

$C_{n_r} = \dfrac{\partial C_n}{\partial \frac{rb}{2V}}$

$C_{n_\beta} = \dfrac{\partial C_n}{\partial \beta}$

$C_{n_{\delta a}} = \dfrac{\partial C_n}{\partial \delta a}$

$C_{n_{\delta r}} = \dfrac{\partial C_n}{\partial \delta r}$

c_t Horizontal tail chord
C_X Axial force coefficient
C_Y Lateral force coefficient

$$C_{y_p} = \frac{\partial C_y}{\partial \frac{pb}{2V}}$$

$$C_{y_q} = \frac{\partial C_y}{\partial \frac{qc}{2V}}$$

$$C_{y_r} = \frac{\partial C_y}{\partial \frac{rb}{2V}}$$

$$C_{y_\beta} = \frac{\partial C_y}{\partial \beta}$$

$$C_{y_{\delta a}} = \frac{\partial C_y}{\partial \widetilde{\delta a}}$$

$$C_{y_{\delta r}} = \frac{\partial C_y}{\partial \delta r}$$

C_z	Normal force coefficient
g	Gravitational constant
h	Center of gravity location in percent mean aerodynamic chord
i_t	Incidence angle of tail
I	Moment of inertia
I_{xx}	Moment of inertia about the x-axis
I_{yy}	Moment of inertia about the y-axis
I_{zz}	Moment of inertia about the z-axis
L	Length or x moment component

$$L_p = \frac{QSb}{I_{xx}} \frac{b}{2V} \frac{\partial C_l}{\partial \frac{pb}{2V}}$$

$$L_r = \frac{QSb}{I_{xx}} \frac{b}{2V} \frac{\partial C_l}{\partial \frac{rb}{2V}}$$

$$L_\beta = \frac{QSb}{I_{xx}} \frac{\partial C_l}{\partial \beta}$$

$$L_{\delta a} = \frac{QSb}{I_{xx}} \frac{\partial C_l}{\partial \delta a}$$

$$L_{\delta r} = \frac{QSb}{I_{xx}} \frac{\partial C_l}{\partial \delta r}$$

l	Rolling moment
l_t	Distance between quarter chords of wing and horizontal tail
l_v	Distance between quarter chords of wing and vertical tail
M	Y moment component

$$M_q = \frac{QS\bar{c}}{I_{yy}} \frac{\bar{c}}{2V} \frac{\partial C_m}{\partial \frac{q\bar{c}}{2V}}$$

$$M_u = \frac{S\bar{c}}{I_{yy}V} \frac{\partial Q C_m}{\partial \frac{u}{U}}$$

$$M_\alpha = \frac{QS\bar{c}}{I_{yy}} \frac{\partial C_m}{\partial \alpha}$$

$$M_{\dot{\alpha}} = \frac{QS\bar{c}}{I_{yy}} \frac{\bar{c}}{2V} \frac{\partial C_m}{\partial \frac{\dot{\alpha}\bar{c}}{2V}}$$

$$M_{\delta e} = \frac{QS\bar{c}}{I_{yy}} \frac{\partial C_m}{\partial \delta e}$$

m	Mass, or pitching moment
m.a.c.	Mean aerodynamic chord
MHz	Megahertz
N	Z moment component

$$N_p = \frac{QSb}{I_{zz}} \frac{b}{2V} \frac{\partial C_n}{\partial \frac{pb}{2V}}$$

$$N_r = \frac{QSb}{I_{zz}} \frac{b}{2V} \frac{\partial C_n}{\partial \frac{rb}{2V}}$$

$$N_\beta = \frac{QSb}{I_{zz}} \frac{\partial C_n}{\partial \beta}$$

$$N_{\delta a} = \frac{QSb}{I_{zz}} \frac{\partial C_n}{\partial \delta a}$$

$$N_{\delta r} = \frac{QSb}{I_{zz}} \frac{\partial C_n}{\partial \delta r}$$

n	Yawing moment
PMARC	Panel Method, Ames Research Center
p	Roll rate, or period
Q	Dynamic pressure
q	Pitch rate
r	Yaw rate
S, S_{ref}	Reference area
S_t	Horizontal tail planform area
S_v	Vertical tail planform area
S_{wing}	Wing planform area
SAM	Surface-to-air missile
u/U	Ratio of change in airspeed to trim airspeed

V	Velocity
V'	Vertical tail volume coefficient in roll
V_H	Horizontal tail volume coefficient
V_V	Vertical tail volume coefficient in yaw
W	Weight

$$X_u = \frac{S}{mV}\frac{\partial QC_X}{\partial \frac{u}{U}}$$

$$X_\alpha = \frac{QS}{m}\frac{\partial C_X}{\partial \alpha}$$

$$X_{\delta e} = \frac{-QS}{m}\frac{\partial C_D}{\partial \delta e}$$

$$Y_p = \frac{QS}{m}\frac{b}{2V}\frac{\partial C_Y}{\partial \frac{pb}{2V}}$$

$$Y_r = \frac{QS}{m}\frac{b}{2V}\frac{\partial C_Y}{\partial \frac{rb}{2V}}$$

$$Y_\beta = \frac{QS}{m}\frac{\partial C_Y}{\partial \beta}$$

$$Y_{\delta a} = \frac{QS}{m}\frac{\partial C_Y}{\partial \delta a}$$

$$Y_{\delta r} = \frac{QS}{m}\frac{\partial C_Y}{\partial \delta r}$$

$$Z_q = \frac{QS}{m}\frac{\bar{c}}{2V}\frac{\partial C_L}{\partial \frac{q\bar{c}}{2V}}$$

$$Z_u = \frac{S}{mV}\frac{\partial QC_z}{\partial \frac{u}{U}}$$

$$Z_\alpha = \frac{QS}{m}\frac{\partial C_z}{\partial \alpha}$$

$$Z_{\dot{\alpha}} = \frac{QS}{m}\frac{\bar{c}}{2V}\frac{\partial C_L}{\partial \frac{\dot{\alpha}\bar{c}}{2V}}$$

$$Z_{\delta e} = \frac{-QS}{m}\frac{\partial C_L}{\partial \delta e}$$

$\bar{Z}$	Distance from pivot to center of gravity
α, alpha	Angle of attack

$$\dot{\alpha} = \frac{\partial \alpha}{\partial t}$$

α_{L_0}	Angle of zero lift
α_{trim}	Angle of attack in the trimmed condition
β, beta	Sideslip angle
δa	Aileron deflection
δe	Elevator deflection
$\delta_{e_{trim}}$	Elevator deflection in the trimmed condition
δr	Rudder deflection
θ, theta	Pitch angle
ϕ, phi	Bank angle
ω	Weight per unit length

Subscripts

LONG	Long chain
M	Model
M+S	Model and support
S	Support
SHORT	Short chain

ACKNOWLEDGMENTS

The staff and faculty of the Naval Postgraduate School Department of Aeronautics and Astronautics are responsible as a whole for making my education an outstanding one. Thank you to all I have come in contact with.

A very special thanks is due to Professor Richard M. Howard. His generosity with his time and seemingly infinite patience go well above and beyond the call of duty. His encouragement and guidance provided me with the motivation to start this project and the endurance to see it through. He would make an outstanding commanding officer.

A very special thanks is also due to Mr. Don Meeks. He is the finest model craftsman and pilot I have come in contact with. His ability to listen open-mindedly to a student's craziest ideas and discuss them in a sensible and reasonable manner make him a true team player.

The biggest thank-you of all goes to the most important person in my life; my wife, Lynne. Her tolerance of the endless hours spent with books instead of her, when she had every right to my time, is truly commendable. Her support throughout my tour here is appreciated more than she knows. She deserves a commendation medal. I love you, Lynne.

I. INTRODUCTION

A. MISSION NEED

Unmanned Aerial Vehicles (UAVs) are gaining acceptance as an integral part of the operations of today's armed forces. Preceding and during Operation Desert Storm, UAVs flew a variety of missions including reconnaissance, targeting for gunfire support, and battle damage assessment. Desert Storm provided the first-ever combat test of Unmanned Aerial Vehicles by U.S. forces [Ref. 1]. Reviews of lessons learned from Desert Shield and Desert Storm reveal the outstanding successes of UAVs.

There are many examples of effective UAV use during the war. In one instance, a commander of a Marine task force was able to monitor UAV imagery of Kuwait as his task force approached the city, revealing the exact reaction of the Iraqi forces to Marine armor, artillery, and troop movements. The Navy used UAVs to search for mines, spot for gunfire support, perform reconnaissance missions for SEAL teams, and search for Iraqi Silkworm sites, command and control bunkers, and anti-aircraft artillery sites. The Marines quickly reacted to an Iraqi attack into Saudi Arabia observed by a UAV and decisively crushed the Iraqi invasion with airborne Cobras and Harriers. The Army provided their Apache pilots with route reconnaissance acquired from UAVs shortly before the Apache missions. Spotting for air strikes and naval gunfire support

became so successful that Iraqi soldiers were seen attempting to surrender to UAVs as they flew overhead [Ref. 2].

UAVs have many advantages over manned aircraft which help account for their effectiveness. First, the cost of a UAV is a very small fraction of the cost of a manned aircraft. The Pioneer, for example, costs approximately $500,000 for the aircraft and $500,000 for the onboard camera, bringing the total cost of the package to a mere one to two percent of the cost of most manned tactical aircraft. UAVs are also extremely flexible with respect to launch platform. They can be launched from small fields, truck beds, and practically any ship in the Navy inventory. UAVs are frequently very hard to detect with radar or infrared systems due to their small size, composite construction, small engines (sometimes electric motors), and their slow speed. UAVs also have an advantage from being unmanned. The aircraft is not limited by the "g" tolerance of a pilot or by pilot fatigue. Finally, the best advantage of all is that when a UAV crashes or is lost to enemy fire, there is no search and rescue mission required, no prisoners of war taken, and no loss of life.

UAVs are not without their problems, however. Acquisition and support programs are relatively new and underdeveloped. This results in a UAV force that is relatively small in number of aircraft, and small and inexperienced in terms of personnel. The Pioneer showed signs of these underlying problems during Desert Storm. Six Pioneers were damaged badly enough to require return to the factory for repair due to no intermediate level maintenance facilities being available. Five Pioneers were lost due to mechanical

malfunction or operator error [Ref. 2]. Due to the small number of available aircraft, losses are very costly and operator errors need to be avoided if possible. Thorough and frequent training through simulation can keep operators performing at their peak.

B. STATEMENT OF OBJECTIVE

To provide realistic simulation for training, accurate aerodynamic data for the aircraft must be available. Aerodynamic parameters of the aircraft can be determined from its physical characteristics, wind tunnel tests, and flight tests of actual or scale models. It is the objective of this work to provide the ground work for determining whether flight test can effectively be used to accurately estimate the static and dynamic stability and control characteristics of a fixed wing UAV. Flying-qualities parameters were estimated using analytic techniques, and the resultant flight dynamics were simulated to provide expected behavior for future test flights.

II. BACKGROUND

A. EVOLUTION OF AN AIRCRAFT

For any aircraft to get from an idea to an actual flying vehicle, properties such as stability and control derivatives, which determine the flying characteristics of the aircraft, must be determined. These derivatives are used to size control surfaces, design flight control systems, and program training devices such as simulators. There are typically three ways to determine or estimate derivatives.

The first method of determining an aircraft's derivatives begins early and continues throughout the design process. This step involves determining derivatives mathematically from physical characteristics of the aircraft. Requiring little more than a few well-educated engineers and some calculators or desktop computers, this method is relatively simple. Derivatives can be reasonably approximated, but must be refined through other methods.

The second method of determining derivatives is through aerodynamic measurements of wind tunnel testing. This method is more complicated than simple pencil and paper calculations due to the necessity for model making and wind tunnel operation, but much better results can be achieved. Derivatives must still be refined, however, due to factors such as scale effects and interference from wind tunnel walls and

supporting hardware. Also, dynamic effects are often difficult to properly account for in most wind tunnels.

The final step approach to determining the derivatives of an aircraft is through flight test. This method is by far the most expensive and complicated way to determine the aircraft's derivatives, but it is also the most precise and complete. Scaled flight test provides a viable option for this third method.

B.   PIONEER UAV

In June 1982, Israeli forces very successfully used UAVs as a key element in their attack on Syria. Scout and Mastiff UAVs were used to locate and classify SAM and AAA weaponry and to act as decoys for other aircraft. This action resulted in heavy Syrian losses and minimal Israeli losses. A year and a half later, the U.S. Navy launched strikes against Syrian forces in the same area with losses much higher for the Navy than those of the Israelis [Ref. 3].

The Commandant of the Marine Corps, General P. X. Kelly, recognized the effectiveness of the Israeli UAVs. Secretary of the Navy John Lehman then initiated development of a UAV program for the U.S. Anxious to get UAVs to the fleet, Secretary Lehman stipulated that UAV technology would be off-the-shelf [Ref. 4]. After the contract award to AAI Corporation of Baltimore, Maryland for the Pioneer UAV, developmental and operational testing took place concurrently. This approach resulted in quick integration of the Pioneer into the fleet. Unfortunately, such quick integration into

the fleet can result in problems identified during operational use which had not been fully explored in the test and evaluation process.

The UAV Office at the Pacific Missile Test Center (PMTC, now the Naval Air Warfare Center, NAWC, Weapons Division, Pt. Mugu) was tasked with Developmental Test and Evaluation of the Pioneer. Testing revealed the following concerns which warranted further investigation [Refs. 5,6]:

1. discrepancies in predicted with flight-tested rate of climb, time to climb, and fuel flow at altitude;

2. apparent autopilot-related pitch instability;

3. tail boom structural failure;

4. severely limited lateral control;

5. slow pitch response causing degraded maneuverability at high gross weights;

6. insufficient testing to determine the effects of the new wing on flight endurance.

The Target Simulation Laboratory at Pt. Mugu was tasked to develop a computer simulation of the Pioneer in order to provide cost-effective training for pilots. Aerodynamic data were needed to provide the stability and control derivatives necessary for the simulation as well as to answer questions concerning basic flying qualities of the Pioneer.

In order to provide support to the research being done at Pt. Mugu and to provide for future UAV project support, a research program was begun at the Naval Postgraduate School (NPS). An instrumented half-scale radio-controlled model of the Pioneer was used

6

for the research at NPS. Research performed included wind tunnel tests, flight tests, and numerical modeling.

Initial NPS research on the Pioneer, performed by Capt. Daniel Lyons, involved a computer analysis of the Pioneer in its original configuration and with a proposed larger tail. A low order panel method (PMARC) was used for the aerodynamic analysis. Static longitudinal and directional stability derivatives, the neutral point, and crosswind limitations were calculated. Drag polars were constructed using the component buildup method for profile drag, and drag reduction measures were considered [Ref. 7].

In conjunction with Capt. Lyons work, Lt. James Tanner conducted wind tunnel tests to determine propeller efficiencies and thrust coefficients for drag studies [Ref. 8]. Lt. Tanner also conducted flight tests to determine power required curves and drag polars [Ref. 8]. Capt. Robert Bray later conducted wind tunnel tests of a 0.4-scale model at Wichita State University to determine static stability and control derivatives [Ref. 9]. Aerodynamic data obtained by Capt. Lyons and Bray have been supplied to PMTC to be used for simulation.

Lt. Jim Salmons performed initial flying qualities flight testing using an onboard data recording system in order to determine static stability parameters. Unfortunately, vibration problems with the onboard recorder rendered much of the data unusable [Ref. 10].

Following up on Lt. Salmons' work, Lt. Kent Aitcheson installed the CHOW-1G telemetry system, designed by Lt. Kevin Wilhelm, in an attempt to alleviate the vibration

problem experienced by Lt. Salmons. The new flight test configuration was used to test static longitudinal and lateral-directional stability characteristics of the Pioneer. The vibration problem experienced by Lt. Salmons was overcome, though not enough data were acquired for a complete and thorough analysis of the Pioneer's characteristics. Much insight was gained, however, concerning instrumentation. Resolution needed to be improved for flight control position indication [Refs. 11,12].

Lt. Paul Koch conducted further flight tests of the Pioneer with the CHOW-1G telemetry system. Static longitudinal stability results from the flight tests correlated well with theoretical predictions and with simulations of a full-scale Pioneer. Electromagnetic interference with the flight control system at the test site resulted in loss of the half-scale model Pioneer before further data collection and analysis could be performed [Ref. 13].

C. PARAMETER ESTIMATION

Parameter estimation is used to derive stability and control derivatives from dynamic flight test data. Lcdr. Robert Graham successfully used the Modified Maximum Likelihood Estimation (MMLE) technique with MATLAB software to analyze simulated and actual flight test data of several aircraft. Analysis of simulated UAV data revealed the effect of signal-to-noise ratio on the estimator, and the need for proper control-surface excitation for a particular response [Ref. 14]. Cdr. Patrick Quinn analyzed flight test data from the Marine Corps BQM-147 UAV using both MMLE and a more robust non-linear model, pEst, and compared the results of the two approaches. Noise was found to be a problem when the system response was in the same general frequency as the noise.

Limited available data and noise at the frequency expected for the system's response prevented a successful resolution of all stability and control derivatives of interest. The pEst model was found to be the estimator of choice when aircraft maneuvers exceed what is generally considered reasonable for linear approximation of flight dynamics [Ref. 15].

While previous work with UAVs at NPS has at times been frustrating, much has been learned, especially concerning the most challenging method of aircraft analysis, flight test. This work initiates the implementation of the lessons learned from previous work into dynamic simulation and flight testing of a generic UAV in order to properly prepare the UAV lab at NPS for further support of future projects and to demonstrate the value of scaled UAV flight test to the fleet.

III. THE AIRCRAFT

A. GENERAL DESCRIPTION

The "Bluebird", shown in Figures 1-3, is a high-wing tricycle-gear radio-controlled airplane. It is constructed of wood, foam, composites, and metal. It is powered by a Sachs-Dolmar 3.7-cubic-inch two-stroke gasoline engine which drives a 24 inch two-bladed wood propeller. It is controlled by a nine-channel pulse-code-modulated Futaba radio operating at 72.710 MHz. To enhance reliability, the Bluebird has two receivers which share control of the aircraft. The left receiver controls the left aileron, elevator, and flap, and engine ignition and onboard electronics package cut-off, while the right receiver controls the right aileron, elevator, and flap, and rudder, nose-wheel steering, and throttle. The Bluebird can fly within visual range for approximately 1.5 hours. Table 1 describes physical specifications of the Bluebird.

B. STABILITY DERIVATIVES

The initial estimates of the stability derivatives of the Bluebird were made using the physical characteristics of the aircraft such as airfoil data , geometric measurements, relative positions of aircraft components, mass, and weight [Refs. 16-19]. The assumed flight condition with the associated aircraft configuration is described in Table 2. Nondimensional stability and control derivatives estimated are shown in Table 3, and

10

dimensional stability and control derivatives estimated are shown in Table 4. MATLAB

programs written for the physical and derivative calculations appear in Appendix A.

TABLE 1
SPECIFICATIONS

Length .... 9.84 ft.
Height .... 3.04 ft.
Wing Airfoil (est.) .... GO 769
Horizontal Stab. Airfoil (est.) .... NACA 4412
S_{wing} (S_{ref}) .... 22.38 ft.^{2}
S_t .... 4.701 ft.^{2}
S_v .... 1.277 ft.^{2}
c .... 1.802 ft.
c_t .... 1.281 ft.
b .... 12.42 ft.
b_t .... 3.67 ft.
b_v .... 1.21 ft.
AR 6.89
AR_t 2.86
AR_v 1.14
V_H 0.6274
V_V 0.0247
V' 0.0023
l_t .... 5.381 ft.
l_v .... 5.381 ft.

TABLE 2
FLIGHT CONDITION/AIRCRAFT CONFIGURATION

Weight .... 57.79 lbs.
I_{xx} .... 12.58 slug*ft^2
I_{yy} .... 13.21 slug*ft^2
I_{zz} .... 19.99 slug*ft^2
Velocity .... 60 mph/88 ft/sec
Altitude .... 800 ft MSL
Density .... 0.002327 slugs/ft^3
Center of Gravity .... 27% of m.a.c.
C_{Ltrim} 0.2866
A.o.A$_{trim}$ .... 3.8 degrees
Elevator$_{trim}$ .... 1.6 degrees
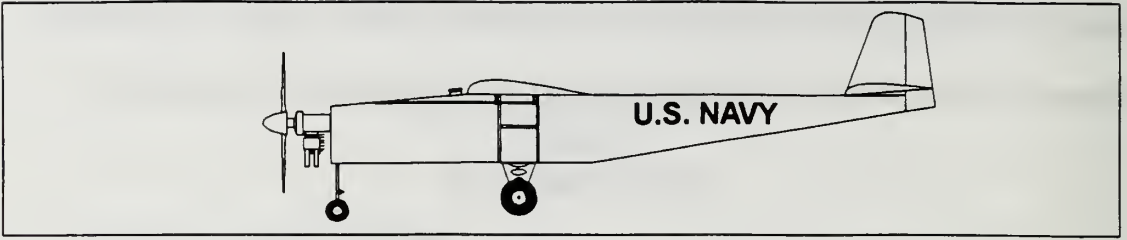
Figure 1
Side View
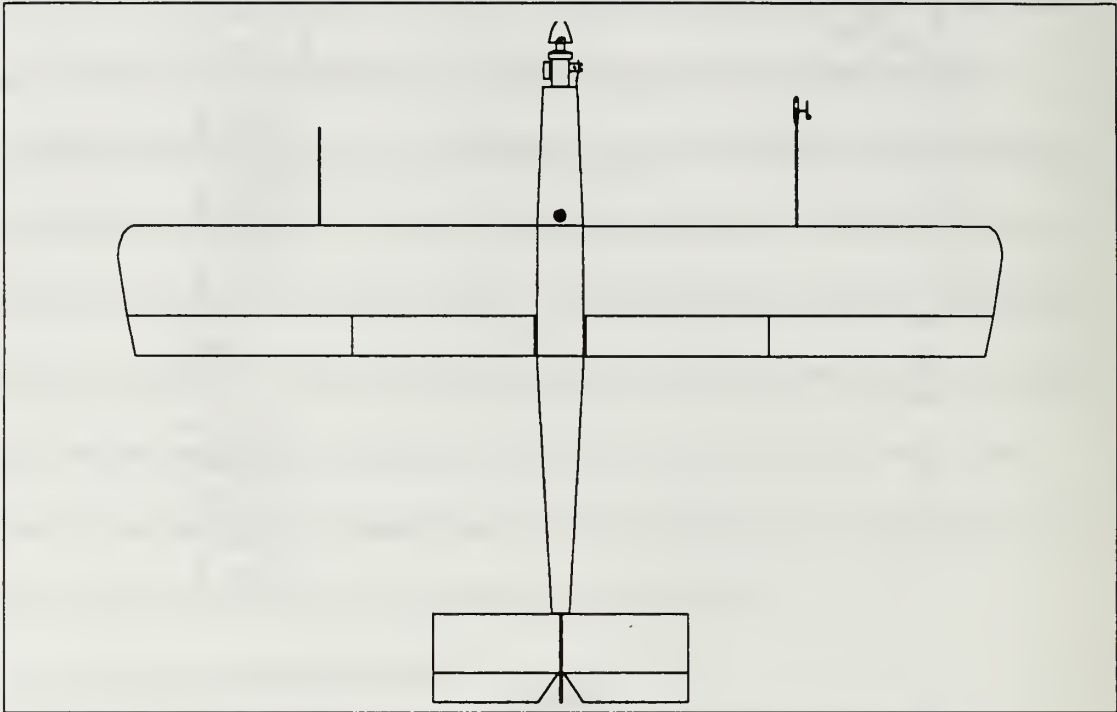
Figure 2
Top View
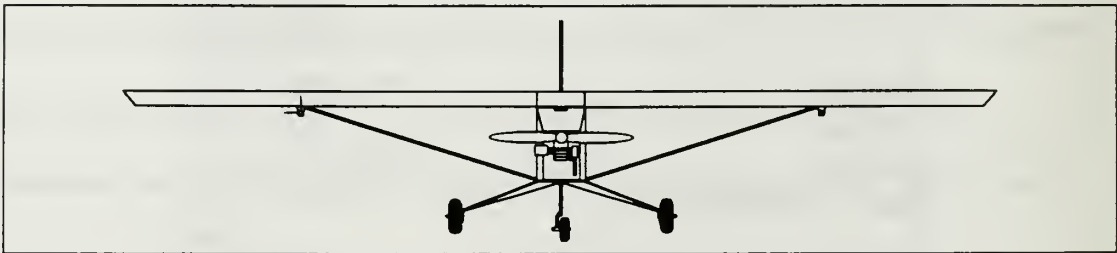
Figure 3
Front View

12

TABLE 3
NONDIMENSIONAL DERIVATIVES

C_L	0.2866	C_D	0.0358
C_{L_α}	4.1417	C_{D_o}	0.0311
$C_{L_{\dot\alpha}}$	1.5787	C_{D_α}	0.1370
C_{m_α}	-1.0636	$C_{m_{\dot\alpha}}$	-4.6790
C_{L_q}	3.9173	C_{m_q}	-11.6918
$C_{L_{\delta e}}$	0.4130	$C_{D_{\delta e}}$	0.0650
$C_{m_{\delta e}}$	-1.2242	C_{y_β}	-0.3100
C_{n_β}	0.0484	C_{l_β}	-0.0330
C_{y_p}	0.0000	C_{n_p}	-0.0358
C_{l_p}	-0.3579	C_{y_r}	0.0967
C_{n_r}	-0.0526	C_{l_r}	0.0755
$C_{y_{\delta a}}$	0.0000	$C_{n_{\delta a}}$	-0.0258
$C_{l_{\delta a}}$	0.2652	$C_{y_{\delta r}}$	0.0697
$C_{n_{\delta r}}$	-0.0326	$C_{l_{\delta r}}$	0.0028
C_{D_q}	0.0000	C_{y_q}	0.0000

TABLE 4
DIMENSIONAL DERIVATIVES

X_u	-0.0914 /sec	X_α	16.7894 ft/sec
$X_{\delta e}$	-7.2961 ft/sec²	Z_u	-0.7312 /sec
Z_α	-468.9852 ft/sec²	$Z_{\dot\alpha}$	1.8146 ft/sec
Z_q	4.5027 ft/sec	$Z_{\delta e}$	-46.368 ft/sec²
M_u	0.0000 /ft*sec	M_α	-29.2559 /sec²
$M_{\dot\alpha}$	-1.3178 /sec	M_q	-3.2928 /sec
$M_{\delta e}$	-33.6730 /sec²	Y_β	-34.8021 ft/sec²
Y_p	0.0000 ft/sec	Y_r	0.7663 ft/sec
$Y_{\delta a}$	0.0000 ft/sec²	$Y_{\delta r}$	-7.8282 ft/sec²
L_β	-6.5787 /sec²	L_p	-5.0281 /sec
L_r	1.0613 /sec	$L_{\delta a}$	52.7966 /sec²
$L_{\delta r}$	0.5589 /sec²	N_β	6.0593 /sec²
N_p	-0.3167 /sec	N_r	-0.4647 /sec
$N_{\delta a}$	-3.2375 /sec²	$N_{\delta r}$	-4.0900 /sec²

C. MOMENTS OF INERTIA

Having accurate moments of inertia is critical to ensuring the accurate prediction of aircraft dynamics. Direct calculation of a model's moments of inertia by consideration of the contributions made by individual parts is impractical and inaccurate. Determination of the moments of inertia by test is much more practical and precise. The changes in a model's moments of inertia due to addition or subtraction of equipment or structure can be calculated directly, thereafter.

In the determination of moments of inertia by test, the aircraft is hung from the ceiling and swung. Using the period exhibited and the principles of compound pendulums, the moments of inertia of the model can be extracted [Ref. 20-21]. In order to calculate the moment of inertia about all axes, the model must be hung from the ceiling and swung three different ways, each such that as the aircraft swings, it is rotating about the axis of interest. The Bluebird was hung by chain and swung as pictured in Figures 4-6. Specifications for the geometry of each test can be found in Appendix B.

Reference 21 provides equation (1) for calculating the moment of inertia of a swinging model.

$$I = \frac{W_{M+S}\bar{Z}_{M+S}}{4\pi^2}p_{M+S}^2 - \frac{W_S\bar{Z}_S}{4\pi^2}p_S^2 - \frac{W_M\bar{Z}_M^2}{g} \qquad (1)$$

W is the weight, $\bar{Z}$ is the distance from pivot to center of gravity, p is the period, and g is the gravitational constant. M and S are subscripts designating either the model or the support.
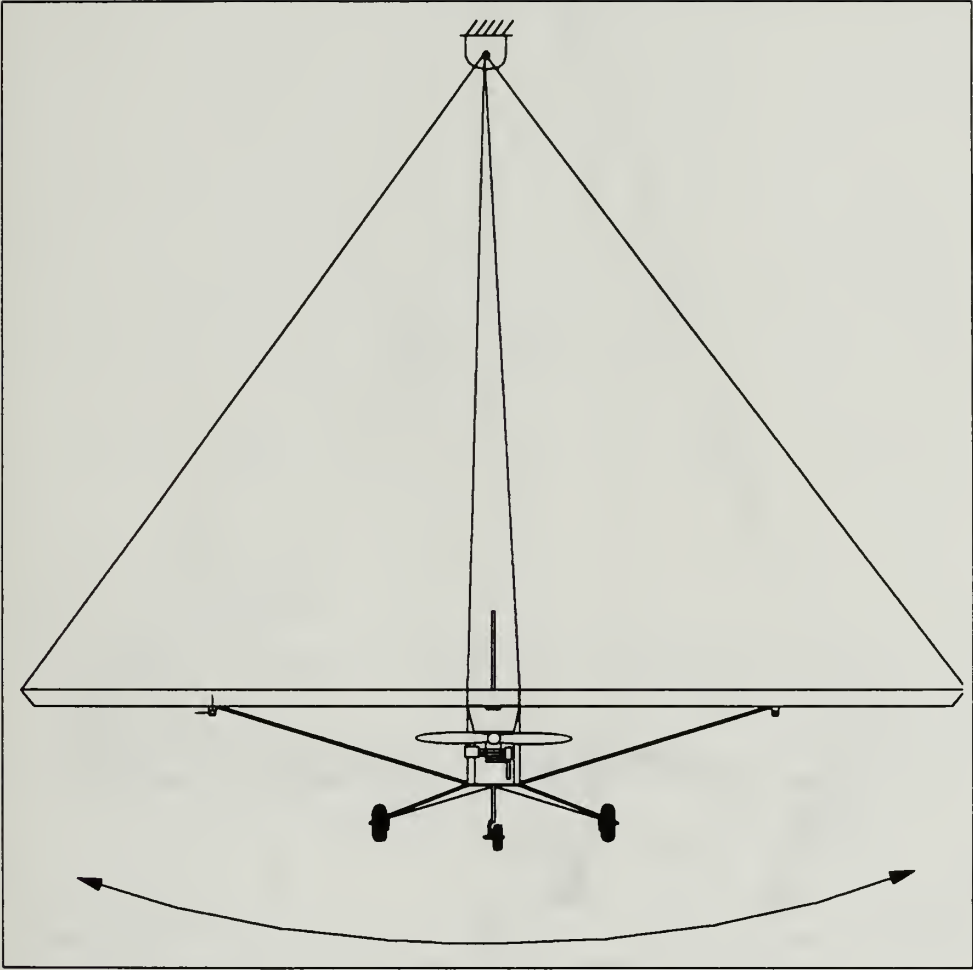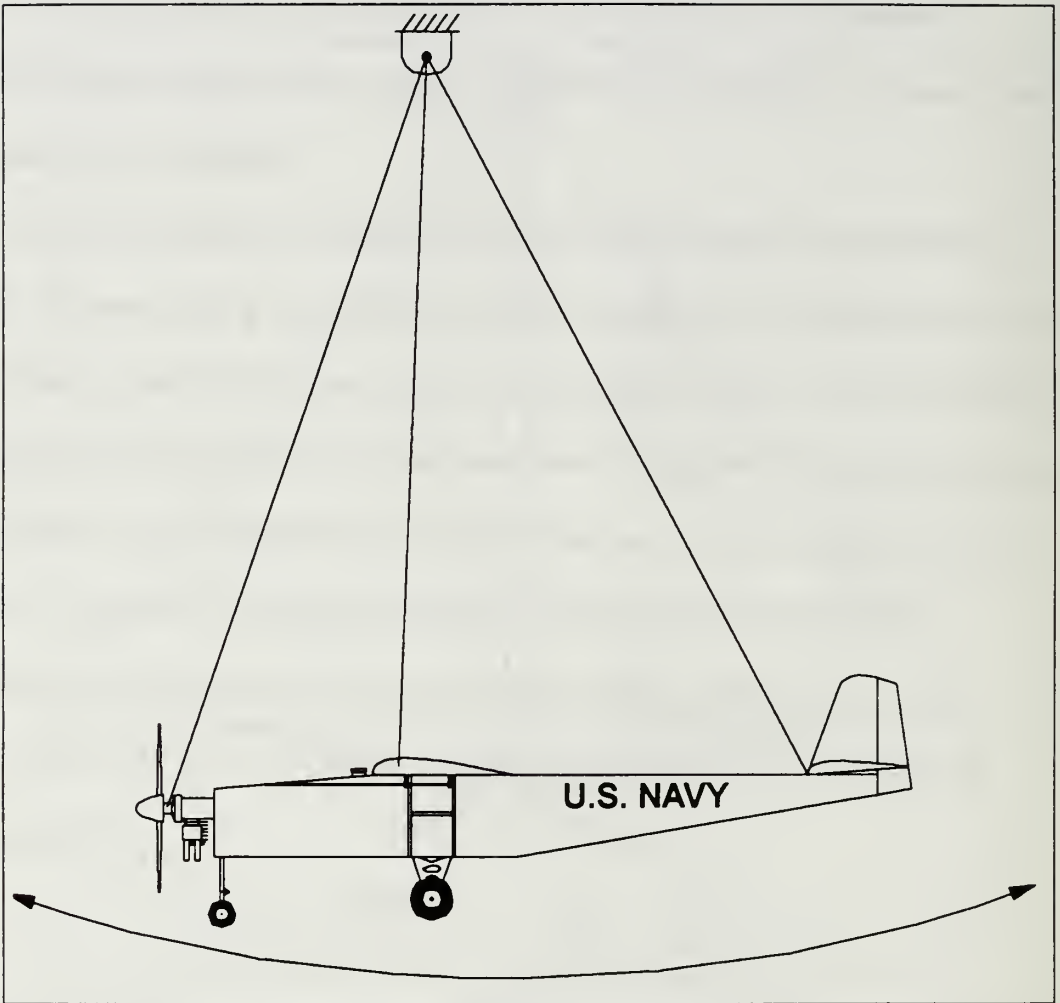
Figure 4
I_{xx} Test (not to scale)

Figure 5
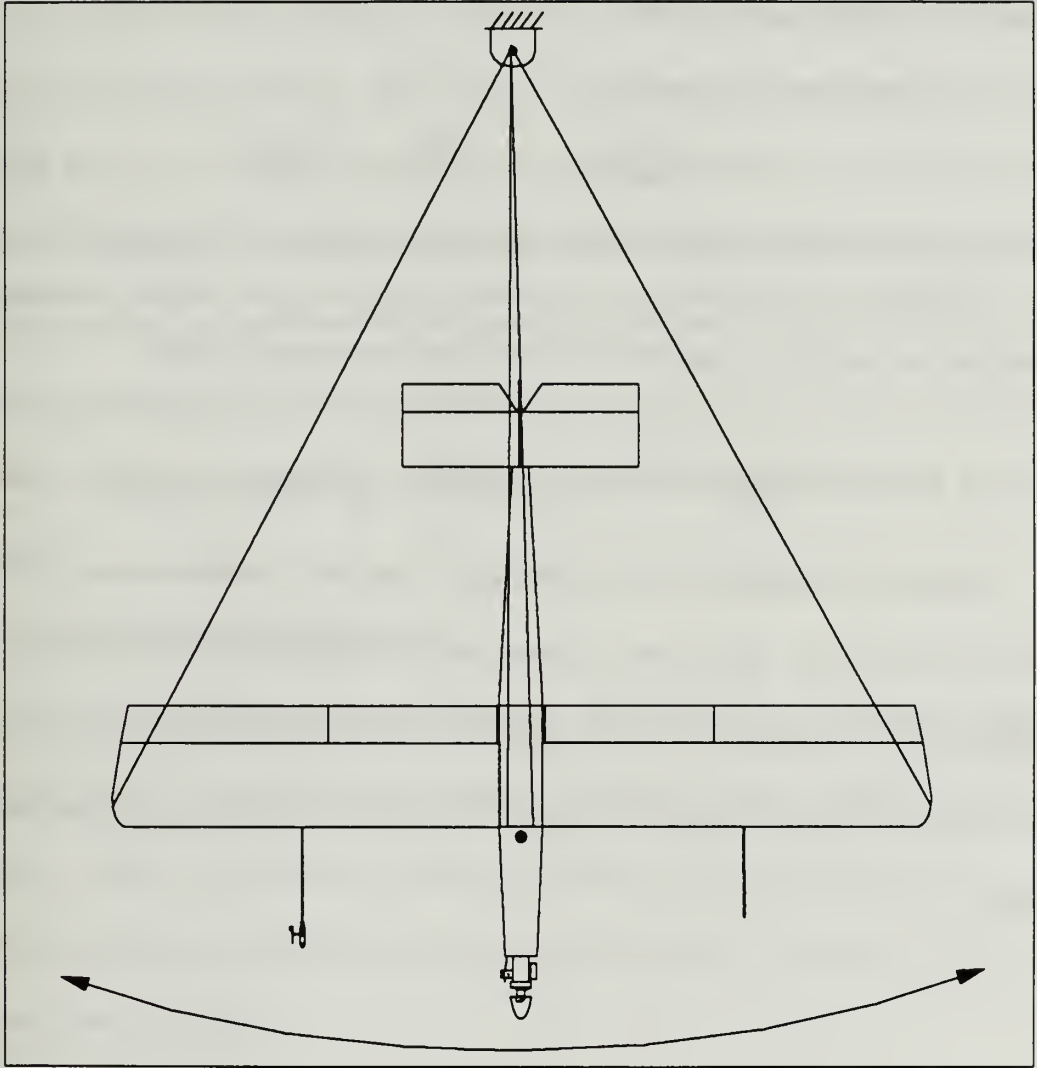I_{yy} Test (not to scale)

16

Figure 6
I_{zz} Test (not to scale)

It was determined that swinging the support (the chains) in the configuration it would be in when supporting the model would not be possible, since the chains would not maintain their positions without the model in place. Equation (1) was therefore manipulated in order to treat the chains as long slender rods and to calculate their moments of inertia as such [Ref. 22].

The new form of equation (1) is

$$I = \frac{W_{M+S}\bar{Z}_{M+S}}{4\pi^2}p_{M+S}^2 - \frac{W_M\bar{Z}_M^2}{g} - \Sigma\frac{(W_S)_i(L_S)_i^2}{3g} \tag{2}$$

where L_S is the length of a chain and the summation is taken over all chains (four in this case). In particular, there were two "long" chains and two "short" chains, all having a weight per unit length ω. Appropriate substitutions were made to yield

$$I = \frac{[W_M + 2\omega(L_{SHORT} + L_{LONG})]\bar{Z}_{M+S}}{4\pi^2}P_{M+S} - \frac{W_M\bar{Z}_M^2}{g} - \frac{2\omega}{3g}\left(L_{SHORT}^2 + L_{LONG}^2\right) \tag{3}$$

Having the equation in this form fixes the values for all variables except $\bar{Z}_{M+S}$, $\bar{Z}_M$, and p_{M+S}. These three variables were measured for each of the three configurations and calculations were made. Four periods were timed during the swing tests, and the tests were repeated ten times. The moments of inertia calculated are shown in Table 2.

IV. PREDICTED DYNAMICS

A. GENERAL

When flight testing an aircraft, it is important to attempt to predict the results of the testing prior to the actual flights. The information provided by the predictions can be used in briefing the pilot as to what to expect from the aircraft and also to avoid any potentially dangerous flight regimes. Longitudinal and lateral-directional dynamics of the Bluebird have been predicted using the stability and control derivatives estimated in chapter three along with computational methods based upon the six equations of motion as described in references 18 and 23. Computational programs were written in MATLAB and appear in Appendix C.

B. LONGITUDINAL DYNAMICS

The MATLAB program named "longnat.m" uses the full (4x4) longitudinal plant and the MATLAB "impulse" function to determine the short and long period natural responses. A diary of the values computed and output by the program provides eigenvalues, damping ratios, and damped and undamped natural frequencies for both modes as shown in Table 5.

TABLE 5
LONGITUDINAL DATA

	Short Period	Long Period
Eigenvalues	-5.083 +/- 4.861i	-0.037 +/- 0.400i
Damping ratio	0.723	0.093
Undamped Natural Frequency	7.03 rad/sec	0.401 rad/sec
Damped Natural Frequency	4.86 rad/sec	0.399 rad/sec

Figures 7 and 8 show the combined short and long period natural response. It can be seen that the short period response is almost completely damped out after only two seconds. Response beyond two seconds is primarily long period. The phugoid mode is seen to be lightly damped.

The short and long period response to a unit step elevator input is determined by using the full (4x4) longitudinal plant and the MATLAB "step" function in the MATLAB program named "stepper.m". Figures 9 and 10 show the short and long period response to a step input. In the first plot, the long period can be seen to be much more heavily excited than the short period mode. Again, it can be seen that the short period response is almost completely damped out after about two seconds. Due to held elevator input, the long-term response is to trim to a new angle of attack, while pitch rate dies out.

The MATLAB program named "n_step.m" uses the full (4x4) longitudinal plant and the MATLAB "step" function to determine the normal acceleration or load factor response to a unit step elevator input. Figure 11 shows the short period normal acceleration response to a unit step input. It should be noted that normal acceleration is defined opposite in sign to load factor. The long-period response is seen to be much
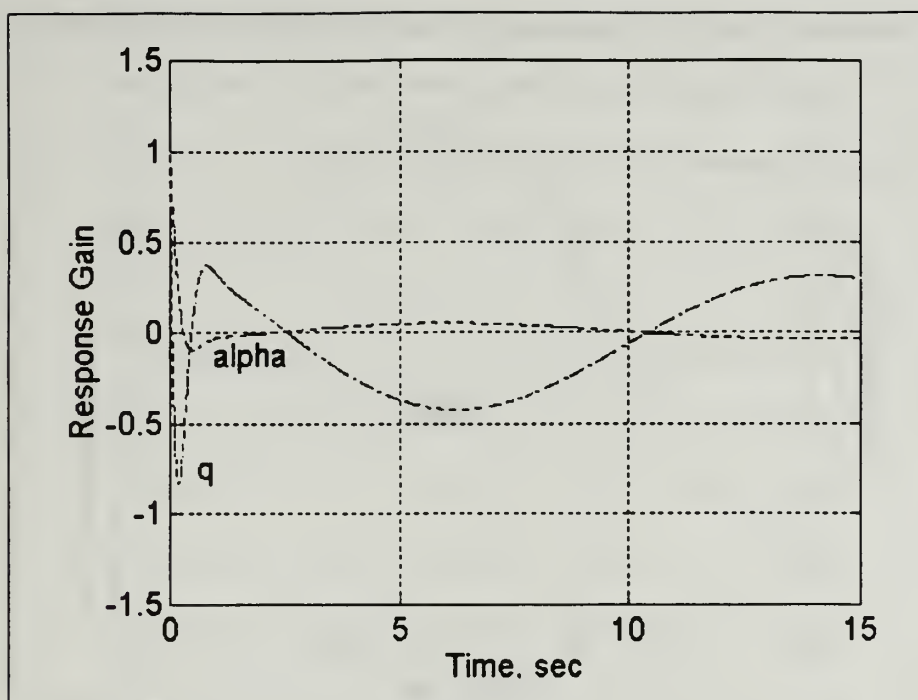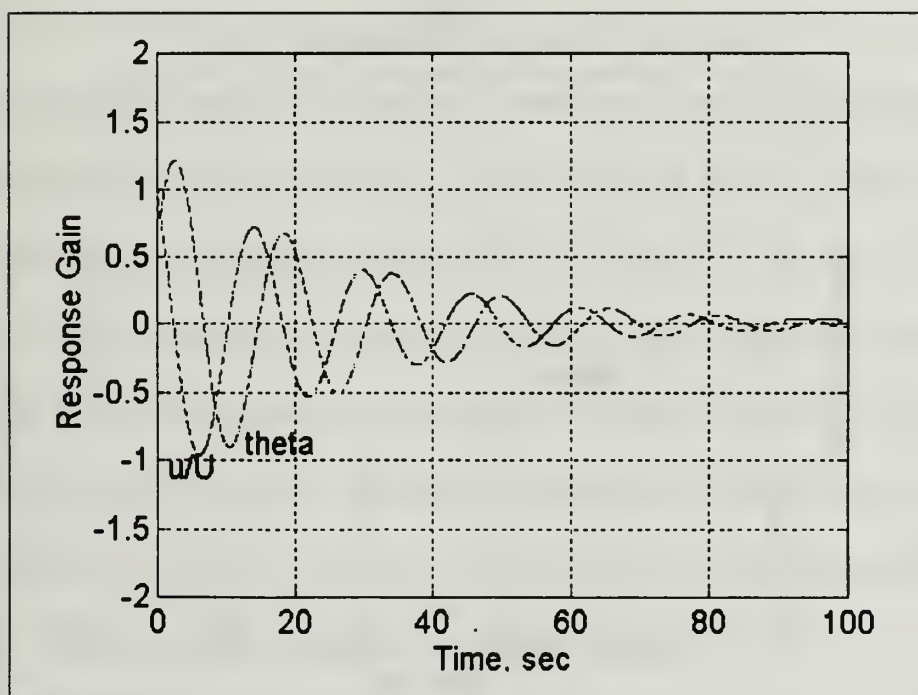
Figure 7
Natural Response (short time)

Figure 8
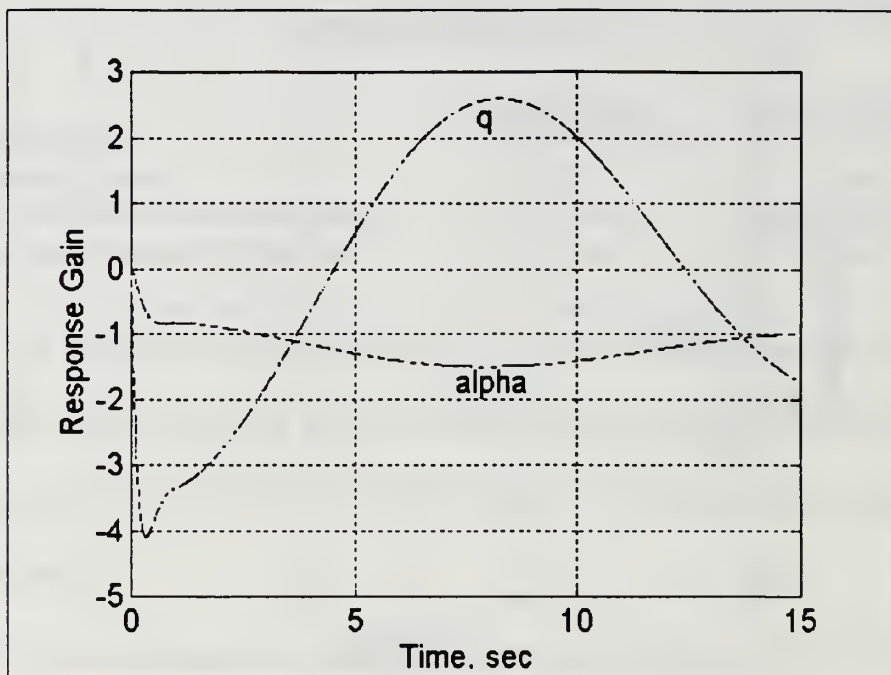Natural Response (long time)

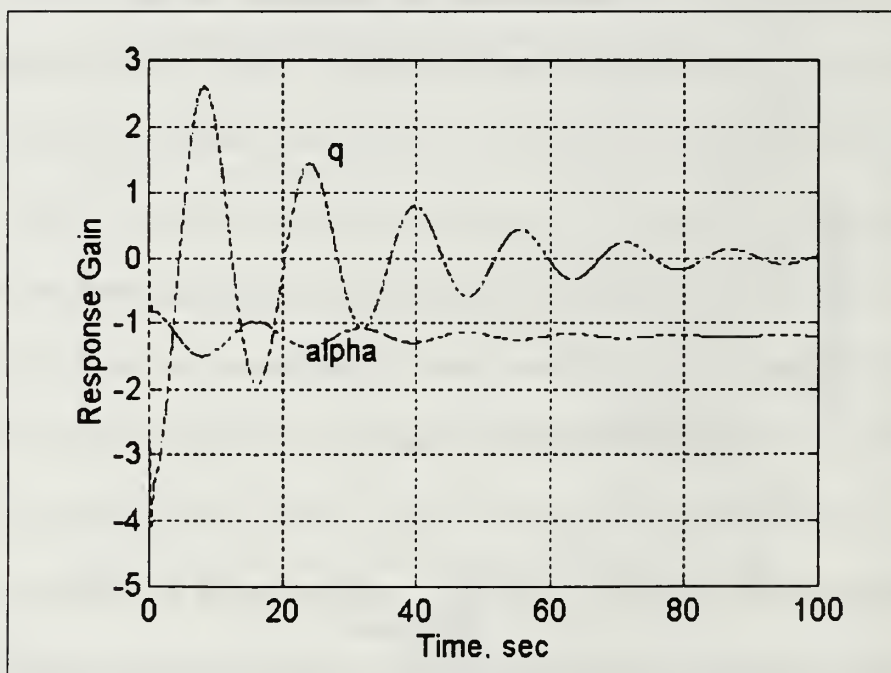Figure 9
Response to Step Input (short time)

Figure 10
Response to Step Input (long time)

more critical than the short-period response in generating large load factors for this aircraft.

Figure 11
Normal Acceleration Response to Step Input

The longitudinal response to given initial conditions is determined using the full (4x4) longitudinal plant and the MATLAB "initial" function in the MATLAB program named "homogen.m". The initial conditions (u/U = .34, alpha = 5 deg, q = 8.8 deg/sec, theta = -0.8 deg) are provided for all states from the step input results after initial dynamics have died out (approximately 15 seconds). Figures 12 and 13 show the longitudinal response to the initial conditions. The response in angle of attack is small while a significant pitch rate is developed in both the short-period and long-period responses. The long-period is again seen to be lightly damped.

The MATLAB program named "doublet.m" uses the full (4x4) longitudinal plant and the transition matrix (using the MATLAB "exponential" function) to find the
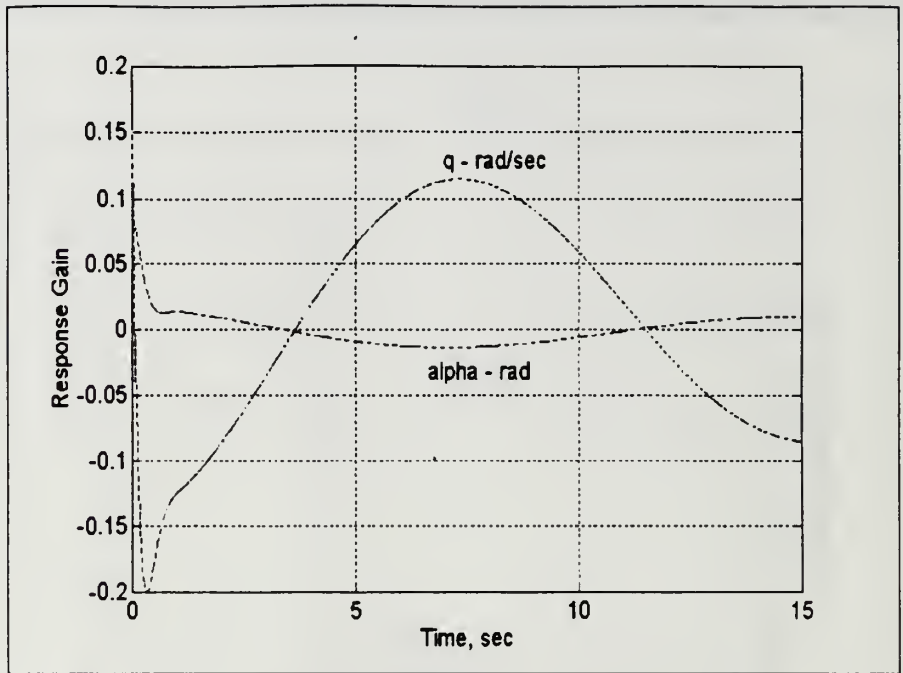
23

Figure 12
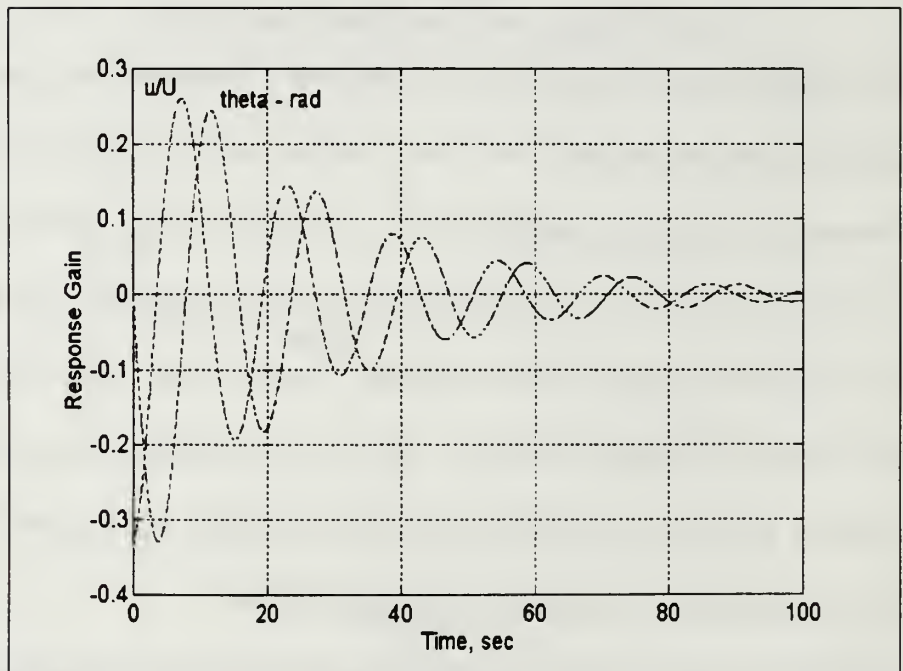Homogeneous Response (short time)

Figure 13
Homogeneous Response (long time)

response to a unit pitch doublet input at approximately the short period damped natural frequency. Figure 14 shows the input pitch doublet, and Figure 15 shows the response. Though the doublet is commonly used to observe only the short-period response, the angle of attack response indicates the long-period response is also excited.

The response (transfer function gain and phase) to a harmonic elevator input is found using the full (4x4) longitudinal plant and the MATLAB "bode" function in the MATLAB program named "sp_bode.m". Figures 16 and 17 show the gains and phase shifts from an elevator frequency sweep. The angle of attack gain can be seen decreasing from a peak at a very low excitation frequency; the short-period response is masked by the long-period gain. In actuality, the low-frequency response is of little interest. Pitch rate shows a maximum gain at approximately 2.4 radians/second corresponding to an elevator cycle period of approximately 2.6 seconds.

The MATLAB program named "n_bode.m" uses the full (4x4) longitudinal plant and the MATLAB "bode" function to find the normal acceleration or load factor response (transfer function gain and phase) to a harmonic input. Figures 18 and 19 show the normal acceleration gains and phase shifts from an elevator frequency sweep. The short and long-period damped natural frequencies can be observed at 4.86 radians/second and 0.399 radians/second respectively where their respective gains peak. While the gain demonstrated at the long-period damped natural frequency is quite significant, the aircraft would not be expected to be excited at that frequency. An excitation near the short-period damped natural frequency is much more likely. Flight test pilots and
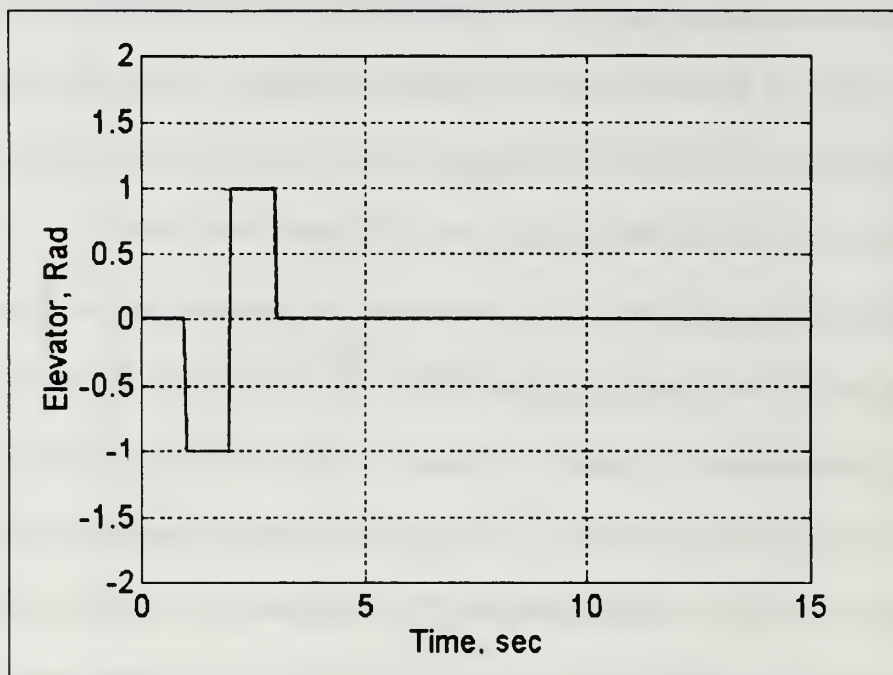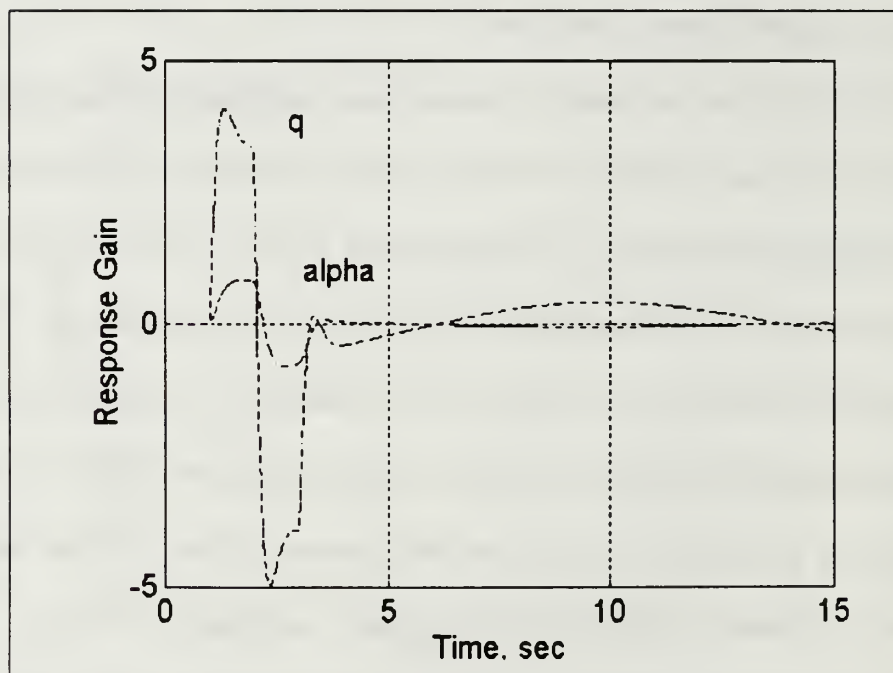
Figure 14
Unit Elevator Doublet Input
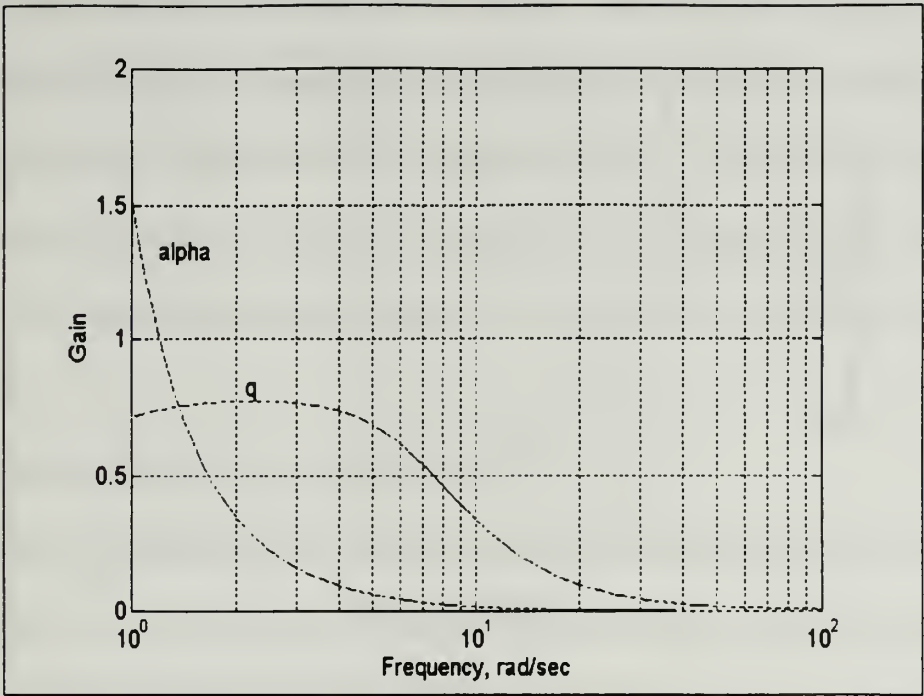

Figure 15
Doublet Response
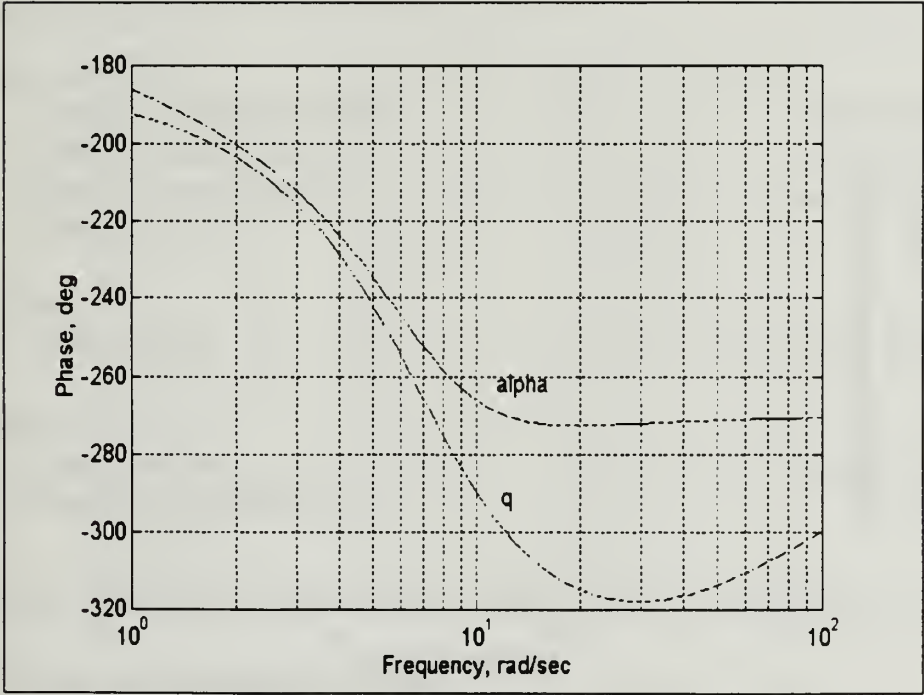
Figure 16
Frequency Response (Gain)
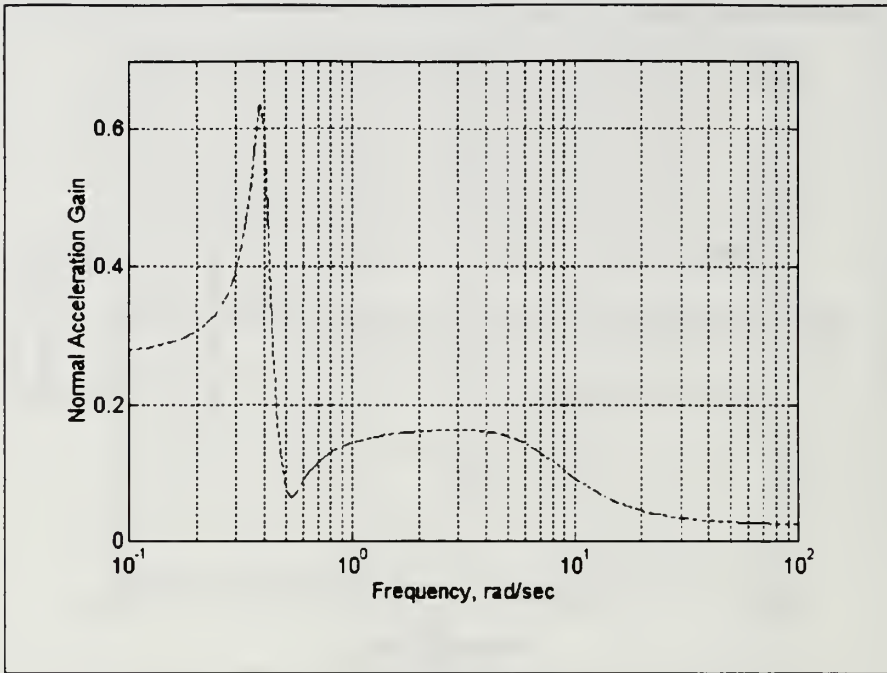

Figure 17
Frequency Response (Phase)

Figure 18
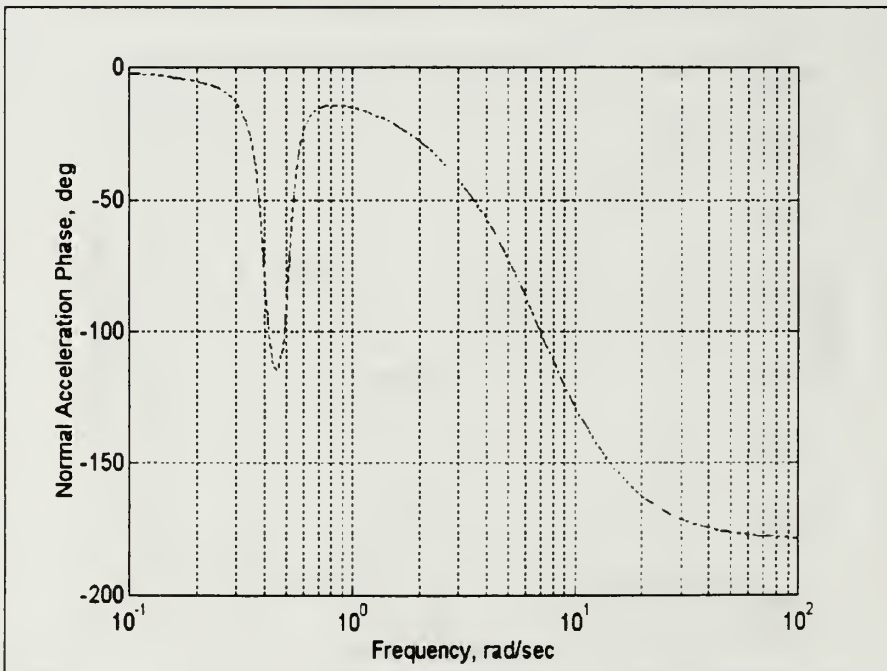Normal Acceleration Response to a Harmonic Input (Gain)

Figure 19
Normal Acceleration Response to a Harmonic Input (Phase)

28

engineers should be aware of the fact that excitation at that frequency will produce approximately 0.15 "g's" per degree of elevator deflection or that it takes a harmonic amplitude of about 6.7 degrees of elevator to produce one "g" of acceleration. The Bluebird has a maximum of 15 degrees of up elevator and 12 degrees of down elevator available. This would equate to approximately -0.8 to +3.2 "g's", which is easily tolerated structurally.

C. LATERAL-DIRECTIONAL DYNAMICS

Undamped natural frequency, damped natural frequency, damped natural period, and damping ratio for the Dutch roll mode; time constant for the roll mode; and time constant and time to double or half for the spiral mode are calculated by the MATLAB program named "lat_dir.m" using the full (4x4) lateral-directional plant. Values calculated are described as follows.

Dutch roll mode:
Undamped natural frequency	2.65 rad/sec
Damped natural frequency	2.62 rad/sec
Damped natural period	2.40 sec
Damping ratio	0.148

Roll mode:
Time constant	0.195 sec

Spiral mode:
Time constant	-29.28 sec
Time to double amplitude	20.29 sec

The Dutch roll mode is observed to be lightly damped. Also, the spiral mode is divergent with a fairly short time to double bank angle.

The MATLAB program named "rudkick.m" uses the full (4x4) lateral-directional plant and the MATLAB "impulse" function to find the response to a unit rudder impulse. The program also finds the bank angle at the end of 100 seconds which is approximately four degrees in the direction of the rudder kick. Figure 20 shows the unit rudder kick response in bank and sideslip angles. Sideslip lags bank angle by approximately 0.6 seconds or 80 degrees of phase and is approximately 60 percent larger in magnitude.

The response to an initial sideslip is determined by the MATLAB program named "sideslip.m" using the full (4x4) lateral-directional plant and the MATLAB "initial" function. Initial conditions for sideslip and bank angle are provided by a steady-sideslip condition where bank angle is ten degrees, and sideslip angle is 13.7 degrees. Figure 21 shows the homogeneous response to the initial sideslip. The lightly damped Dutch roll mode can be seen by observing the oscillations of both bank angle and sideslip angle, while the divergent spiral mode can be observed by the increasing bank angle.

The MATLAB program named "roll.m" uses the full (4x4) lateral-directional plant and the MATLAB "bode" function to find the roll angle response (transfer function gain and phase) due to a harmonic aileron input. Figures 22 and 23 show the roll angle gains and phase shifts from the harmonic aileron input. The maximum high-frequency roll angle gain is seen to occur at approximately 2.8 radians/second which corresponds to an aileron input period of approximately 2.2 seconds.
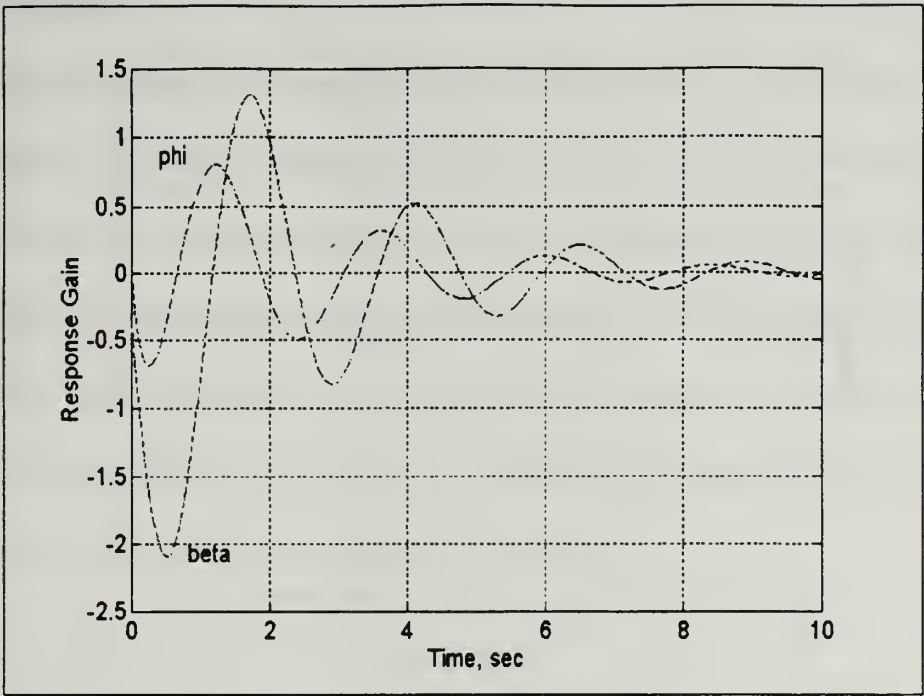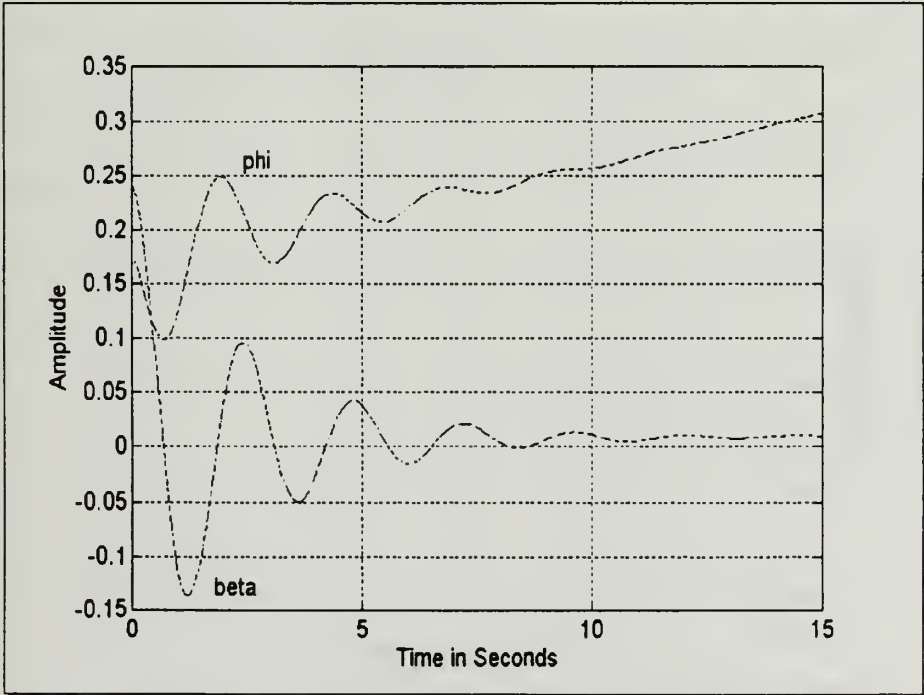
Figure 20
Unit Rudder Kick Response

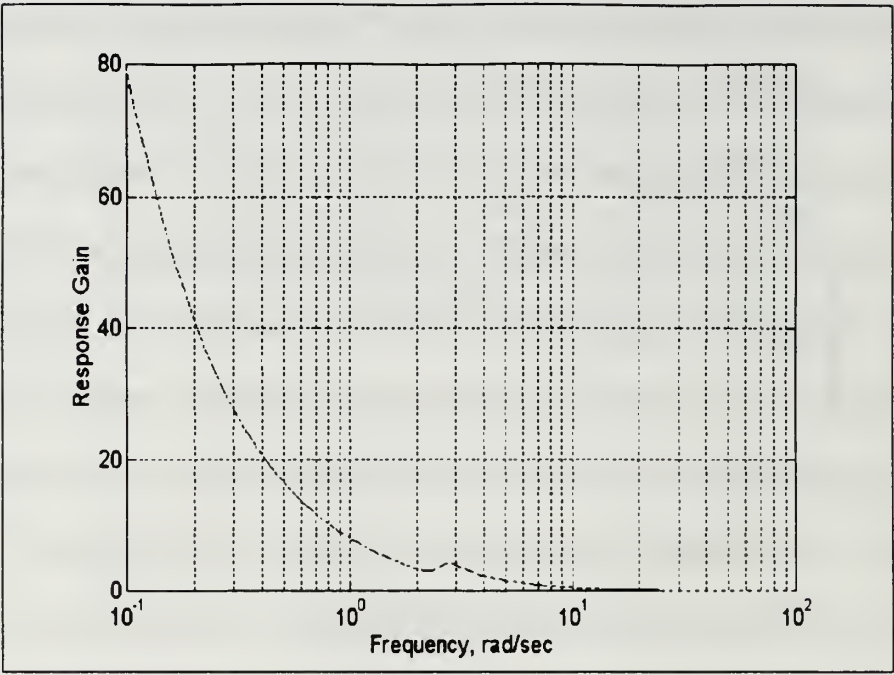Figure 21
Homogeneous Response to an Initial Sideslip

31

Figure 22
Roll Angle Gain due to a Harmonic Aileron Input
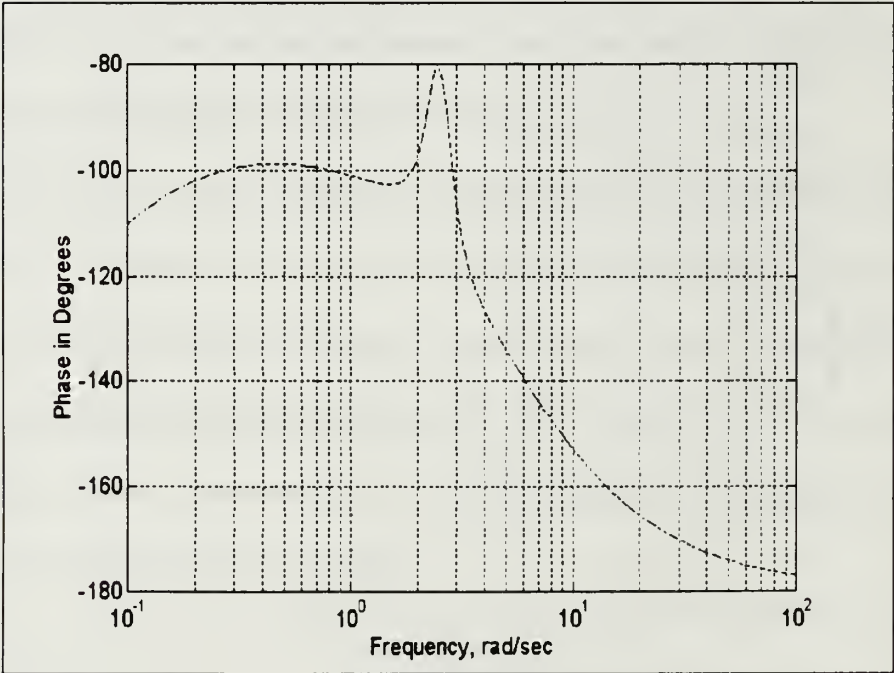
Figure 23
Roll Angle Phase Shift due to a Harmonic Aileron Input

32

D.   REMARKS

Analysis has been conducted for the most common modes. The Bluebird demonstrates no particularly dangerous flying qualities. Particular characteristics of the Bluebird's behavior worth noting include a very heavily damped short period longitudinal mode, a lightly damped phugoid mode, a lightly damped Dutch roll mode, and a divergent spiral mode. Additional analysis could be easily done by analogy to those modes all ready analyzed. Further analysis might include, for example, the response to a step aileron input, aileron doublet, or elevator impulse ("stick rap").

V. FLIGHT TEST

A. TEST DESCRIPTION

The relative positions of an aircraft's center of gravity and neutral point are critical to the aircraft's longitudinal stability and handling qualities. In order for a conventional (aft tail) aircraft to be statically stable, its center of gravity must be forward of its neutral point. The farther the center of gravity is in front of the neutral point (relative to the chord length), the more statically stable the aircraft is. As the center of gravity is moved aft beyond the neutral point, the aircraft becomes statically unstable and more maneuverable.

As an aircraft's center of gravity is moved aft toward the neutral point, less and less change in elevator trim is required to achieve steady, level flight for a given change in airspeed. This fact can be used to experimentally determine the aircraft's neutral point. Reference 23 provides equation (4) which describes the relationship between change in pitching moment coefficient with change in coefficient of lift and the required change in elevator deflection with change in coefficient of lift.

$$\frac{dC_m}{dC_L} = -V_H \bullet C_{L_{t_{\delta e}}} \bullet \frac{d\delta e}{dC_L} \tag{4}$$

As the center of gravity moves aft and approaches the neutral point, dC_m/dC_L approaches zero. Since V_H and $C_{L_{\delta e}}$ are constants, $d\delta e/dC_L$ must also approach zero.

34

In order to determine the neutral point by flight test, the aircraft must be flown at various centers of gravity. At each particular center of gravity, the aircraft is trimmed at several airspeeds (coefficients of lift). Each airspeed and the corresponding elevator deflection are recorded. Plots are then generated showing elevator deflection versus coefficient of lift at each center of gravity tested. A line is then best fit through the data points for each center of gravity. The slope of this line represents $d\delta e/dC_L$ for that particular center of gravity. Finally, $d\delta e/dC_L$ versus center of gravity is plotted. A best fit line is then drawn through these data points. Using the best fit line just drawn, the center of gravity where $d\delta e/dC_L$ equals zero is the aircraft's neutral point.

B. INSTRUMENTATION

In order to acquire the airspeed of the Bluebird, a simple, commercially-available airspeed indicator was installed. The Digicon TT-01 Tele Tachometer/ASI senses the spinning of a small wind-driven propeller blade using a cadmium disulphide optical sensor. The frequency of the changes in light intensity sensed is transmitted to a hand-held receiver which converts the frequency to airspeed which can be read directly in real-time. The manufacturer's claimed accuracy is +/- 0.5 feet per second. The airspeed indicator was installed on the left wing of the Bluebird by mounting it on the end of a boom which extended approximately 18 inches (approximately 80 percent of c-bar) in front of the leading edge of the wing.

Measuring elevator trim was done in an indirect manner. The flight control transmitter has a digital display which can show elevator trim on a generic scale of -100 to

100. Prior to flight test, elevator deflection in degrees was measured for various trim settings, and the relationship between transmitter displayed trim number and actual degrees of elevator deflection was determined. This calibration allowed for the determination of elevator deflection in degrees during post flight analysis.

C. TEST PROCEDURES

In order to fly the Bluebird at various centers of gravity, an access panel in the aft fuselage of the aircraft was modified to accept added weights. The aircraft was then configured with various amounts of weight and the location of the center of gravity determined for each configuration. Centers of gravity were determined by weighing each wheel with a strain-gage balance.

A total of seven flights were flown at various centers of gravity. Flights were kept short in order to minimize the shift in the center of gravity due to fuel burn. The location of the center of gravity was determined both before and after the flight, and the average center of gravity was used for calculations. Shifts in center of gravity during testing were kept to one percent or less of the wing chord.

Each flight consisted of 12 passes at various airspeeds. Airspeed and trim setting for each pass were recorded for post flight analysis. Additionally, air pressure, air temperature, and aircraft weight were noted in order to calculate coefficient of lift.

Post flight analysis of the data was conducted in accordance with the procedures described in Section A, Test Description. The resulting graphs are shown in Figures 24-31.
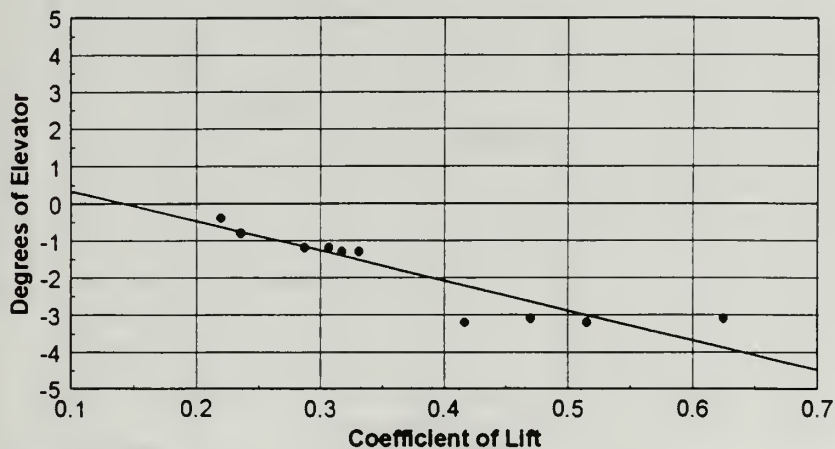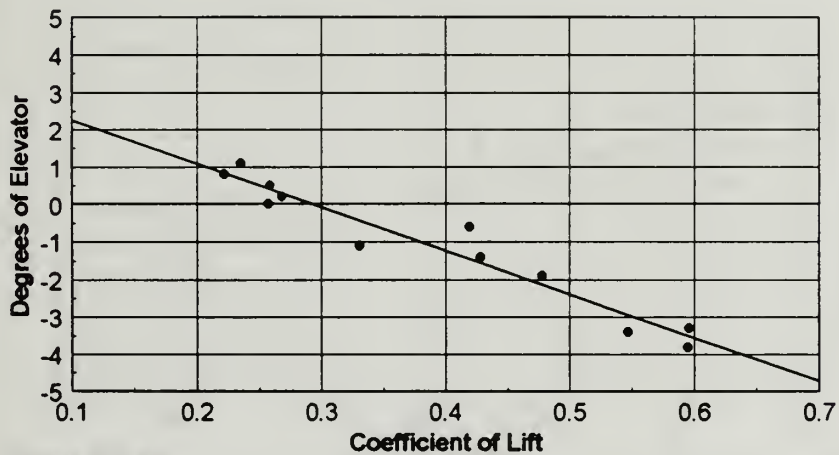
Figure 24
Flight 1 of 7

Figure 25
Flight 2 of 7

C.G. = .2868
04 MAR 94, Flight 1

Slope = -7.461591
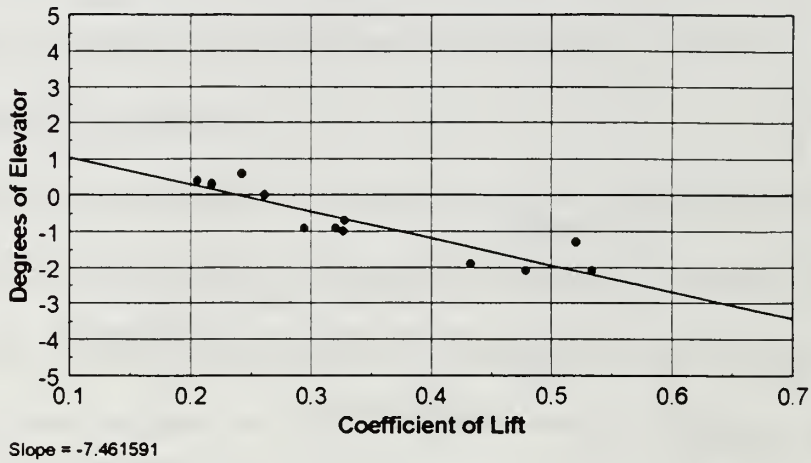
Figure 26
Flight 3 of 7

C.G. = .3198
04 MAR 94, Flight 2

Slope = -8.834435
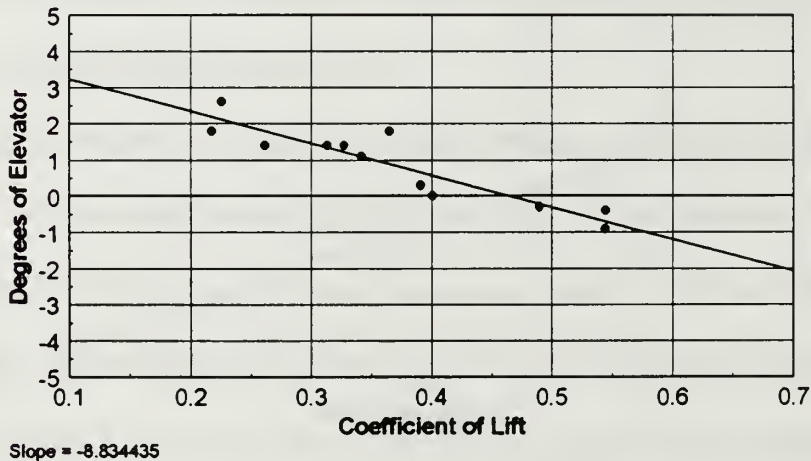
Figure 27
Flight 4 of 7
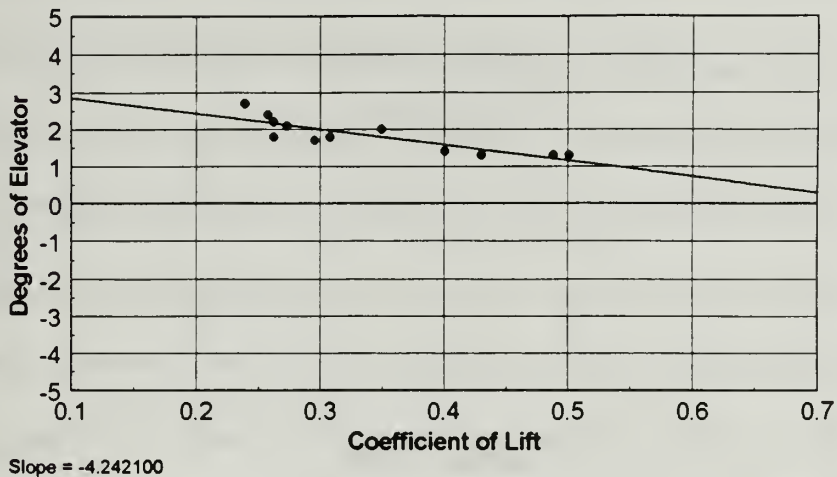
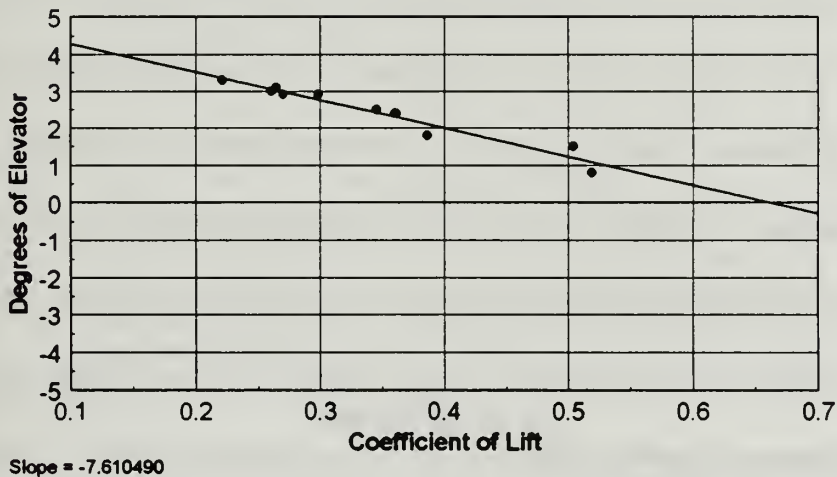Figure 28
Flight 5 of 7

Figure 29
Flight 6 of 7
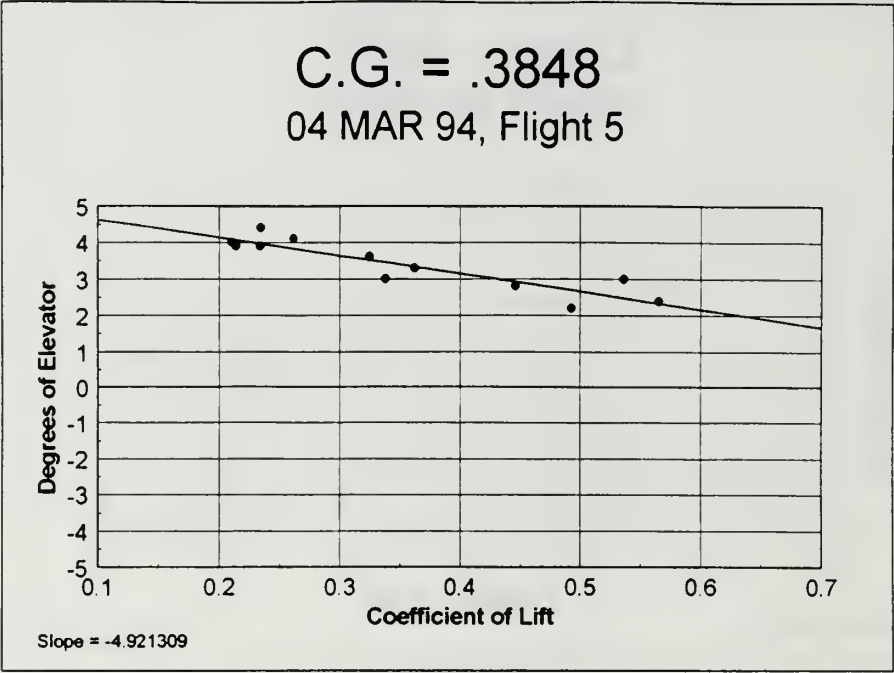
Figure 30
Flight 7 of 7
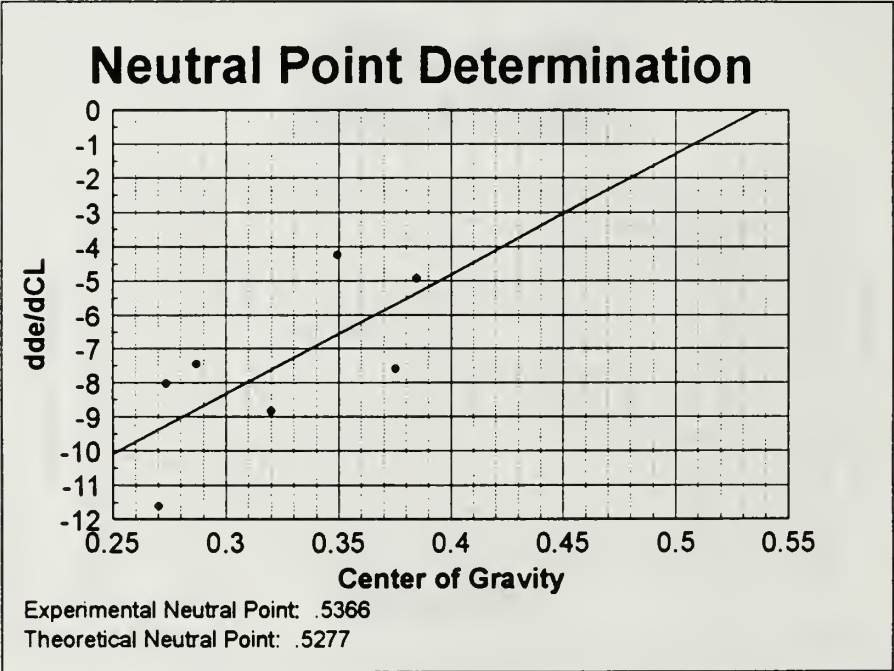
Figure 31
All Flights

D.   RESULTS

The neutral point estimated by flight test was found to be about 54 percent of the mean aerodynamic chord. The neutral point estimated through conventional calculations was approximately 52.8 percent of the mean aerodynamic chord.

While such a close match between the neutral point locations found by each method is highly encouraging, one must not overlook the scatter in the data presented in Figure 31. Assuming a normal distribution of the data, there is a 68 percent confidence that the experimentally determined neutral point is within five percent of the wing mean aerodynamic chord of the location determined experimentally. Such data scatter is unacceptable for accuracies required, and the tests will be repeated when the improved instrumentation under development comes on line.

For the flight testing done, two sources of potential error are of particular interest. First, it was very difficult to ensure a perfectly level pass of the aircraft at each particular airspeed. The pilot was positioned on the ground and the plane was flying approximately one hundred feet above him. This is not an optimum vantage point for the pilot. Ideally, the pilot would like to be elevated (such as in a tower) such that the aircraft is at eye level for each pass. Future plans include using an altitude-hold autopilot to maintain the desired trim conditions. Also, due to wind gusts and possibly small unintentional changes in aircraft attitude, the airspeed was not always steady, and therefore somewhat difficult to read consistently. This second problem will be overcome by the improved data acquisition system.

VI. SUMMARY

A determination of the moments of inertia by the component contribution method was decided to be too cumbersome for analysis of the complete aircraft. Moments of inertia were found through a compound pendulum analysis, and appear reasonable. Future changes to the configuration of the aircraft can be accounted for by considering the contribution of the component added, removed, or relocated.

Initial estimates of stability and control derivatives were made by conventional aircraft-design-type methods. Such methods involve considering characteristics of the aircraft such as lift-curve slopes of airfoils and the locations of particular aircraft components relative to each other. Programs were written in MATLAB in such a manner that future changes to the aircraft or different flight conditions can be accounted for quickly and accurately. The initial estimates of the derivatives can be used in the preliminary design of a flight controller.

The initial estimates of the stability and control derivatives were used to predict the dynamic response of the aircraft to several different excitations. MATLAB programs were written to predict the dynamics, and any future modifications to the aircraft or flight conditions can be accounted for easily. Several characteristics of the aircraft's responses are worth noting. First, the short period longitudinal response was found to be heavily damped. Little or no evidence of the short period response can be observed beyond

approximately two seconds. Second, the long period longitudinal response was found to be lightly damped. The long period response can still be observed relatively easily after 100 seconds. Similarly, the Dutch roll mode is also fairly lightly damped and can be observed easily for ten to 15 seconds. Finally, the spiral mode was found to be divergent with a time to double bank angle of approximately 20 seconds. While this mode is not particularly dangerous for a radio controlled aircraft which is flown visually (open loop), the pilot should be aware of this tendency of the aircraft in order to avoid trim problems. It is also recommended that flight controller designs incorporate bank angle feedback for wing leveling.

The neutral point of the aircraft was found to be 53 to 54 percent of the wing mean aerodynamic chord by two different methods. The data collected through flight test were somewhat scattered; it is estimated that the neutral point location is known within +/- five percent of the wing mean aerodynamic chord with a confidence of about 68 percent. Further flight testing with improved instrumentation is recommended to raise the confidence of the neutral point estimation. It is recommended that flight tests with improved instrumentation continue to verify or update all predicted stability and control derivatives.

APPENDIX A: MATLAB PROGRAMS USED TO ESTIMATE STABILITY AND CONTROL DERIVATIVES

1. blbrdfc1.m

```
% Eric J. Watkiss
% AA0810 Thesis
% File for Bluebird data which change with flight condition
% blbrdfc1.m
% Last Update:  02 MAR 94

g = 32.174;                  % Accelleration due to gravity
Wlmg = 24.02                 % Weight on left main in lbs
Wrmg = 23.91                 % Weight on right main in lbs
Wng = 11.07                  % Weight on nose gear in lbs

Umph = 60                    % Flight speed in miles per hour
Ufps = 88.0                  % Flight speed in feet per second

rho = .002327                % Air density in slugs/(cubic ft)

Ixx = 12.58                  % Moment of inertia about x-axis
Iyy = 13.21                  % Moment of inertia about y-axis
Izz = 19.99                  % Moment of inertia about z-axis
Ixz = 0                      % Assumed!!!!!!!!!!!!!!!!!!!!!!!

LD = 8;                      % Lift to drag ratio

thetanaut = 0;               % Initial pitch angle
```

2. bluebird.m

```
% Eric J. Watkiss
% AA0810 Thesis
% File for Bluebird data which are fixed
% bluebird.m
% Last Update:  02 MAR 94


ac = .479;                      % Aileron chord in ft.
ai = 3;                         % distance from centerline to
%                                   inner edge of aileron in ft.
alpha0l = -6.5*pi/180;          % a.o.a. for zero lift (radians)ao = 6;
%                                   distance from centerline to
%                                   outer edge of aileron in ft.
b = 12.42;                      % Span of wing in ft
bt = 3.67;                      % Span of horizontal tail in ft.
bv = 1.208;                     % Height of vertical tail in ft.
cbar = 1.802;                   % Mean aerodynamic chord (m.a.c.)
%                                   in feet
CLalphaafw = 5.443;             % Lift curve slope of wing
%                                   airfoil (GO 769) in per
%                                   radian
CLalphaaft = 5.587;             % Lift curve slope of horizontal
%                                   tail airfoil (NACA 4412) in per
%                                   radian
CLalphaafv = 2*pi;              % Lift curve slope of vertical
%                                   tail airfoil (flat plate) in per
%                                   radian
CMac = -.06;                    % Coefficient of moment about
%                                   aero. ctr. (GO 769)
ct = 1.281;                     % m.a.c. of horizontal tail in ft.
c4tail = 7.878;                 % Location of quarter chord of
%                                   horizontal tail in feet from
%                                   firewall
c4wing = 2.497;                 % Location of quarter chord of
%                                   wing in feet from firewall
da0dde = .625;                  % Section flap effectiveness
%                                   for 33% flap (elevator)
%                                   Abbott and Doenhoff p. 190
da0ddr = .675;                  % Section flap effectiveness
%                                   for 38% flap (rudder)
%                                   Abbott and Doenhoff p. 190
deda = .4;                      % Downwash angle derivative
```

```
%                          estimated from Perkins/Hage
Df = 1;                    % Depth of fuse. in ft.
e0 = 0;                    % Assumed epsilon naught
ee = .8;                   % Assumed span efficiency factor
g = 32.174;                % gravitational constant
hac = .245;                % Location in percent chord of
%                            aero. ctr. (NACA 4412)
it = 4.83*pi/180;          % Incidence angle of hor. tail
lewing = 2.047;            % Location of leading edge of wing
%                            in feet from firewall
letail = 7.557;            % Location of leading edge of
%                            horizontal tail in feet from
%                            firewall
mg = 37.595/12;            % Location of main gear in ft
%                            from firewall
ng = .75/12;               % Location of nose gear in ft
%                            from firewall
S = 22.380;                % Reference (wing) area in sq. ft.
Sr = .547;                 % Rudder area in sq. ft.
St = 4.701;                % Horizontal tail area in sq. ft.
Sv = 1.277;                % Vertical tail area in sq. ft.
Wf = .67;                  % Width of fuse. in ft.
ybar = b/4;                % Spanwise location of m.a.c.
zv = .5;                   % Vert. tail height to m.a.c.
%                            (estimated)
Zwf = .5;                  % Verticle height of wing
%                            above fuse. C.L. in ft.
```

3. dderiv.m

```
% Eric J. Watkiss
% AA0810 Thesis
% File to calculate dimensional derivatives
% dderiv.m
% Last Update:  12 FEB 94

% Run nondimensional derivative program
ndderiv

% Calculate dynamic pressure
qbar = .5*rho*Ufps^2;                    % ft lbs

Malpha = CMalpha*qbar*S*cbar/Iyy;        % per second^2

Mq = CMq*(cbar/(2*Ufps))*qbar*S*cbar/Iyy;
                                         % per second

Malphadot = CMalphadot*(cbar/(2*Ufps))*qbar*S*cbar/Iyy;
                                         % per second

Xu = -2*CD*qbar*S/(m*Ufps);              % per second

Zu = -2*CL*qbar*S/(m*Ufps);              % per second

Zalphadot = CLalphadot*(cbar/(2*Ufps))*(qbar*S/m);
                                         % ft per second

Zq = CLq*(cbar/(2*Ufps))*(qbar*S/m);     % ft per second

Mu = 0;                                  % per ft second

Xde = -1*CDde*qbar*S/m;                   % ft per second^2

Zde = -1*CLdelta*qbar*S/m;               % ft per second^2

Mde = CMde*qbar*S*cbar/Iyy;              % per second^2

Xalpha = (CL - CDalpha)*qbar*S/m;        % ft per second^2

Zalpha = -1*(CLalphaw+CD)*qbar*S/m;      % ft per second^2
```

47

```
YB = CyB*qbar*S/m;                          % ft/second^2

LB = ClB*qbar*S*b/Ixx;                      % 1/second^2

NB = CnB*qbar*S*b/Izz;                      % 1/second^2

Yp = Cyp*b*qbar*S/(2*Ufps*m);               % ft/sec

Yr = Cyr*b*qbar*S/(2*Ufps*m);               % ft/sec

Lp = Clp*(b/(2*Ufps))*qbar*S*b/Ixx;         % 1/sec

Np = Cnp*(b/(2*Ufps))*qbar*S*b/Izz;         % 1/sec

Lr = Clr*(b/(2*Ufps))*qbar*S*b/Ixx;         % 1/sec

Nr = Cnr*(b/(2*Ufps))*qbar*S*b/Izz;         % 1/sec

Ydr = -1*Cydr*qbar*S/m;                     % ft/sec^2

Yda = 0;                                    % ft/sec^2

Ldr = Cldr*qbar*S*b/Ixx;                    % 1/sec^2

Lda = Clda*qbar*S*b/Ixx;                    % 1/sec^2

Ndr = Cndr*qbar*S*b/Izz;                    % 1/sec^2

Nda = Cnda*qbar*S*b/Izz;                    % 1/sec^2

Malphaprime = Malpha + Malphadot*(Zalpha/Ufps);
Mqprime = Mq + Malphadot;
Mdeprime = Mde + Malphadot*(Zde/Ufps);
```

4. godallas.m

```
% Eric J. Watkiss
% AA0810 Thesis
% File to get values of dimensional and nondimensional derivatives
% godallas.m
% Last Update:  04 FEB 94

!del bluebird.dia
diary bluebird.dia
diary on

% Run programs to calculate derivatives
dderiv

% Nondimensional Derivatives
CL
CD
CD0
CLalphaw
CMalpha
CDalpha
CLalphadot
CMalphadot
CLq
CMq
CLdelta
CDde
CMde
CyB
CnB
ClB
Cyp
Cnp
Clp
Cyr
Cnr
Clr
Cyda
Cnda
Clda
Cydr
Cndr
```

Cldr
CDq
Cyq

% Longitudinal Dimensional Derivatives
Xu
Xalpha
Xde
Zu
Zalpha
Zalphadot
Zq
Zde
Mu
Malpha
Malphadot
Mq
Mde

% Lateral/Directional Dimensional Derivatives
YB
Yp
Yr
Yda
Ydr
LB
Lp
Lr
Lda
Ldr
NB
Np
Nr
Nda
Ndr

diary off

5. ndderiv.m

```
% Eric J. Watkiss
% AA0810 Thesis
% File to calculate nondimensional derivatives
% ndderiv.m
% Last Update:  12 FEB 94

% Load Bluebird data with flight condition
physcalc

% Calculate coefficients of lift and drag
CL = W/(.5*rho*Ufps^2*S);
CD = CL/LD;

% Calculate lift curve slope of wing in per radian
CLalphaw = CLalphaafw/(1+CLalphaafw/(pi*ee*AR));

% Calculate lift curve slope of horizontal tail in per radian
CLalphat = CLalphaaft/(1+CLalphaaft/(pi*ee*ARt));

% Calculate lift curve slope of vertical tail in per radian
CLalphav = CLalphaafv/(1+CLalphaafv/(pi*ee*ARv));

% Calculate change in hor. tail lift with change in elevator
dcLtdde = da0dde * CLalphat;         % per radian

% Calculate change in vert. tail lift with change in rudder
dcLvddr = da0ddr * CLalphav;         % per radian

% Calculate zero lift pitching moment
CM0 = CMac + VH * CLalphat * (it + e0);

% Calculate CMalpha in per radian
CMalpha = CLalphaw*((h-hac)-VH*(CLalphat/CLalphaw)*(1-deda));

% Calculate change in aircraft lift with change in elevator
CLdelta = dcLtdde*(St/S);     % per radian

% Calculate chng in aircraft pitching moment w. chng in elevator
CMde = -1*VH*dcLtdde;      % per radian

% Calculate angle of attack and elevator angle for trimmed flight
```

```
%
%        CM = CM0 + CMalpha*alpha + CMde*de
%        Cl = CLalphaw*alpha + CLdelta*de
%
%         _                    _   _     _      _      _
%       | CLalphaw   CLdelta    | | alpha |    | CL     |
%       |                       | |       | =  |        |
%       |_CMalpha     CMde_____| |__ de _|    |_-CM0_|
%
%              A        *    X    =    C
%
A = [ CLalphaw  CLdelta
      CMalpha    CMde  ];
C = [   CL
     -1*CM0 ];
X = inv(A)*C;
atrim = X(1,1);                 % trim a.o.a. in radians
etrim = X(2,1);                 % trim elevator in radians

% Calculate change in yawing moment with change in rudder
% "rudder power"
% assumes VF/Vinfinity = 1
Cndr = -1*VV*dcLvddr;       % in per radian

% Calculate CnB contribution from vert. tail
% CnB = CLalphav*VV*(VF/Vinfinity)^2*(1-dsigma/dbeta)
% assumes VF/Vinfinity = 1 and dsigma/dbeta = 0
CnB = CLalphav*VV;% in per radian

% Calculate change in rolling moment with change in sideslip

% First calculate dihedral contribution from wing
% Raymer p. 439
ClBwf = -1.2*sqrt(AR)*Zwf*(Df+Wf)/b^2;
ClBw = ClBwCL*CL+ClBwf;

% Next calculate contribution from fin
% ClBv = -1*Clalphav*Vprime*(VF/Vinfinity)^2*(1-dsigma/dbeta)
% Assume VF/Vinfinity = 1 and dsigma/dbeta = 0
ClBv = -1*CLalphav*Vprime;          % in per rad

% Combine ClBg and ClBv into ClB
ClB = ClBw + ClBv;   % in per rad
```

```matlab
% Calculate "aileron power", Clda
% See Smetana pp. 139-141
Cldatau = Cldatauo - Cldataui;
Clda = Cldatau*tau;    % in per radian

% Calculate change in yawing moment w. aileron deflection
Cnda = 2*K*CL*Clda;          % in per radian

% Calculate side force due to yaw
% By Smetana p. 107
CyB = -.31;     % in per radian

% Calculate side force due to rudder
Cydr = CLalphav*taur*Sv/S; % in per radian

% Calculate side force due to aileron
% By Smetana, p. 138
Cyda = 0;

% Calculate rolling moment due to rudder
Cldr = Cydr*zv/b;       % in per radian

% Calculate change in drag due to change in elevator
% Smetana pp. 95-100
% Using Figure 26 at 8 degrees aoa
CDde = ((.155-.047)/(20*pi/180))*St/S;       % in per radian

% Calculate change in drag with change in aoa
% Smetana pp. 64-65
% Assuming dCD0/dalpha is negligible
CDalpha = 2*CL*CLalphaw/(pi*ee*AR);     % in per radian

% Calculate change in pitching moment w.r.t. alphadot
% Smetana pp. 78-81, etat assumed = 1
CMalphadot = -2*CLalphat*deda*(ltprime/cbar)*...
(lt/cbar)*(St/S);         % in per radian

% Calculate change in lift with pitch rate
% Smetana pp. 82-85
% Neglecting wing contribution, assuming etat = 1
CLq = 2*(lt/cbar)*CLalphat*(St/S);  % in per radian
```

% Calculate change in lift with alphadot
% Smetana pp. 75-76
CLalphadot = -1*CMalphadot/(lt/cbar);   % in per radian

% Calculate change in pitching moment w. pitch rate
% Smetana pp. 87-88
% Assuming etat = 1
CMq = -2*(cbar/4-h)*abs(cbar/4-h)*CLalphaw/(cbar^2) - ...
2*(lt/cbar)^2*CLalphat*(St/S);   % in per radian

% Calculate roll damping
% Smetana pp. 122-125
% Neglecting contribution from vertical tail
Clp = -.475*(AR+4)/(2*pi*AR/CLalphaw+4);   % in per radian

% Calculate change in yawing moment due to rolling
% Smetana pp. 126-129
% Neglecting contribution from vertical tail
Cnp = -1*CL/8;   % in per radian

% Calculate change in side force with yaw rate
% From Schmidt p. 3-23
% Assume etat = 1
Cyr = 2*VV*CLalphav;   % in per radian

% Calculate change in rolling moment w. yaw rate
% Schmidt p. 3-24
% Tail contribution
Clrv = (zv/b)*Cyr;   % in per radian
% Wing contribution
Clrw = CL/4; % in per radian
% Total
Clr = Clrv + Clrw;   % in per radian

% Calculate yaw damping
% Schmidt p. 3-25
% Tail contribution
Cnrv = -1*(lv/b)*Cyr; % in per radian
% Wing contribution from Smetana p. 136
CD0 = CD-CL^2/(pi*ee*AR);
Cnrw = -.02*CL^2-.3*CD0; % in per radian
% Total
Cnr = Cnrv + Cnrw;   % in per radian

```
% The following 3 derivatives are negligible and taken to be 0
CDq = 0;        % in per radian
Cyq = 0;        % in per radian
Cyp = 0;        % in per radian

% A few misc. calculations

% Static Margin/Neutral Point
statmar = CMalpha/(-1*CLalphaw)
hn = statmar + h
```

6. physcalc.m

```
% Eric Watkiss
% AA0810 Thesis
% File to calculate physical considerations
% physcalc.m
% Last Update:  04 FEB 94

% Load fixed Bluebird data
bluebird

% Load flight condition
blbrdfc1

% Calculate aircraft weight
W = Wlmg + Wrmg + Wng;

% Calculate aircraft mass
m = W/g;

% Calculate aspect ratio of wing
AR = b^2/S;

% Calculate aspect ratio of hor. tail
ARt = bt^2/St;

% Calculate aspect ratio of vert. tail
ARv = bv^2/Sv;

% Calculate longitudinal center of gravity
h = ((ng*Wng + mg*(Wlmg+Wrmg))/W-lewing)/cbar;

% Calculate "tail length" from c.g. to horizontal tail a.c.
% same for horizontal and vertical
lt = c4tail - (lewing + h*cbar);
lv = lt;

% Calculate "tail length" from c/4 wing to c/4 tail
ltprime = c4tail - c4wing;

% Calculate hor. tail volume coefficient
VH = lt*St/(S*cbar);
```

```
% Calculate vert. tail volume coefficient (yaw)
VV = lv*Sv/(b*S);

% Calculate vert. tail volume coefficient (roll)
Vprime = zv*Sv/(b*S);

% Unit antisymmetrical angle of attack for outer and inner
% edge of aileron (See Smetana p. 141)
antisymo = ao/(b/2);
Cldatauo = .74;
antisymi = ai/(b/2);
Cldataui = .23;
cacw = ac/cbar;
tau = .52;

% for yawing moment due to aileron, see p. 142, Smetana
eta = ai/(b/2);
K = -.17;

% for side force due to rudder deflection, see Smetana p. 145
vratio = Sr/Sv;
taur = .62;

% for rolling moment due to sideslip, See Raymer, Fig. 16.21, p. 439
ClBwCL = -.04;
```

APPENDIX B: MOMENT OF INERTIA CALCULATIONS

For the formula

$$I = \frac{[W_M + 2\omega(L_{SHORT} + L_{LONG})]\bar{Z}_{M+S}}{4\pi^2}P_{M+S} - \frac{W_M\bar{Z}_M^2}{g} - \frac{2\omega}{3g}\left(L_{SHORT}^2 + L_{LONG}^2\right)$$

the following data were used for extraction of the moments of inertia.

Fixed values:

Weight of the model,	W_M = 58.45 lbs
Weight per unit length of chain,	ω = 0.06133 lbs/ft
Length of short chain,	L_{SHORT} = 13.00 ft
Length of long chain,	L_{LONG} = 15.00 ft
Gravitational constant,	g = 32.1472 ft/sec^2
(adjusted for latitude and elevation)	

Variable values:

I_{xx}: Distance from pivot to center of gravity
of model and support, $\bar{Z}_{M+S}$ = 12.95 ft
Distance from pivot to center of gravity
of model, $\bar{Z}_M$ = 13.33 ft
Average period of model and support, P_{M+S} = 4.109 sec

I_{yy}: Distance from pivot to center of gravity
of model and support, $\bar{Z}_{M+S}$ = 12.01 ft
Distance from pivot to center of gravity
of model, $\bar{Z}_M$ = 12.35 ft
Average period of model and support, P_{M+S} = 3.976 sec

I_{zz}: Distance from pivot to center of gravity
of model and support, $\bar{Z}_{M+S}$ = 12.49 ft
Distance from pivot to center of gravity
of model, $\bar{Z}_M$ = 12.81 ft
Average period of model and support, P_{M+S} = 4.077 sec

APPENDIX C: MATLAB PROGRAMS USED TO ESTIMATE AIRCRAFT DYNAMICS

A. LONGITUDINAL DYNAMICS

1. longnat.m

```
% Determines the short and long period natural response
% using the full longitudinal plant

clear
dderiv
!del longnat.dia
diary longnat.dia

% Inertial Matrix
in  = [Ufps          0          0 0;
        0      Ufps-Zalphadot 0 0;
        0       -1*Malphadot  1 0;
        0           0         0 1];

% Aircraft Matrix
an = [Ufps*Xu    Xalpha      0       -1*g*cos(thetanaut);
       Ufps*Zu   Zalpha  Ufps+Zq    -1*g*sin(thetanaut);
       Ufps*Mu   Malpha    Mq              0;
        0          0        1              0];

a   = inv(in)*an;
b   = [1; 1; 1; 1];
c   = eye(size(a));
d   = [0; 0; 0; 0];

t = 0:.01:100;

[y,x,t]  = impulse(a,b,c,d,1,t);

clg
figure(1)
%plotting alpha and q, short period
```

59

```
plot(t,y(:,2));axis([0 15 -1.5 1.5]);grid;gtext('alpha')
hold on
plot(t,y(:,3));gtext('q')
xlabel('Time, sec');ylabel('Response Gain')
%title('Natural Response')
hold off
pause

figure(2)
%plotting u/U and theta, phugoid
plot(t,y(:,1));axis([0 100 -2 2]);grid;gtext('u/U')
hold on
plot(t,y(:,4));gtext('theta')
xlabel('Time, sec');ylabel('Response Gain')
%title('Natural Response');
hold off

damp(eig(a))

diary off
```

2. stepper.m

```
% Determines the short and long period step response
% using the full longitudinal plant

clear
dderiv

% Inertial Matrix
in = [Ufps      0      0 0;
        0  Ufps-Zalphadot 0  0;
        0   -1*Malphadot  1  0;
        0       0      0  1];

% Aircraft Matrix
an = [Ufps*Xu   Xalpha   0     -1*g*cos(thetanaut);
      Ufps*Zu   Zalpha  Ufps+Zq -1*g*sin(thetanaut);
      Ufps*Mu   Malpha   Mq          0;
        0        0       1          0]];

% Control Matrix
bn = [Xde  Zde  Mde  0]';

a   = inv(in)*an;
b   = inv(in)*bn;
c   = eye(size(a));
d   = [0 0 0 0]';

t = 0:.01:100;

[y,x,t]  = step(a,b,c,d,1,t);

clg
figure(1)
%plotting alpha and q, short period
plot(t,y(:,2))
axis([0 15 -5 3])
grid;gtext('alpha')
hold on
plot(t,y(:,3));gtext('q')
xlabel('Time, sec');ylabel('Response Gain')
%title('Short Period Step Response')
hold off
```

61

```
pause

figure(2)
%plotting u/U and theta, phugoid
plot(t,y(:,1))
axis
grid;gtext('u/U')
hold on
plot(t,y(:,4));gtext('theta')
xlabel('Time, sec');ylabel('Response Gain')
%title('Long Period Step Response');
hold off
pause

figure(3)
%plotting alpha and q, long period
plot(t,y(:,2))
grid;gtext('alpha')
hold on
plot(t,y(:,3));gtext('q')
xlabel('Time, sec');ylabel('Response Gain')
%title('Long Period Step Response')
hold off
```

3.   n_step.m

```
%   This program uses STEP function to determine
%   normal acceleration response to a unit step input

clear
dderiv

% Inertial Matrix
in  = [Ufps      0      0  0;
        0  Ufps-Zalphadot 0  0;
        0   -1*Malphadot  1  0;
        0      0      0  1];

% Aircraft Matrix
an = [Ufps*Xu   Xalpha   0      -1*g*cos(thetanaut);
      Ufps*Zu   Zalpha  Ufps+Zq -1*g*sin(thetanaut);
      Ufps*Mu   Malpha   Mq           0;
        0        0      1            0];

% Control Matrix
bn = [Xde  Zde  Mde  0]';

a   = inv(in)*an;
b   = inv(in)*bn;
c   = [ Zu  Zalpha  Zq  0 ];
d   = Zde;

t   = 0:0.05:15;

[y,x,t]  = step(a,b,c,d,1,t);

for i = 1:length(t)
   y2  = y/32.174*pi/180;
end

% plotting g's/deg
plot(t,y2);grid
xlabel('Time, sec');ylabel('Normal Acceleration: g s/deg')
%title('Acceleration Response to Unit Step')
```

4.   homogen.m

```
% Determines the short and long period homogeneous response
% using the full longitudinal plant

clear
dderiv

% Inertial Matrix
in = [Ufps        0        0 0;
        0  Ufps-Zalphadot 0  0;
        0   -1*Malphadot   1   0;
        0        0         0  1];

% Aircraft Matrix
an = [Ufps*Xu   Xalpha    0      -1*g*cos(thetanaut);
       Ufps*Zu   Zalpha  Ufps+Zq -1*g*sin(thetanaut);
       Ufps*Mu   Malpha   Mq            0;
          0        0      1              0];

% Control Matrix
bn = [Xde  Zde  Mde  0]';

a  = inv(in)*an;
b  = inv(in)*bn;
c  = eye(size(a));
d  = [0 0 0 0]';

t = 0:.01:100;

[y,x,t]  = step(a,b,c,d,1,t);

x0  = y(find(t==15),:);
x0 = x0/x0(2)*5/57.3
[y,x,t]  = initial(a,b,c,d,x0,t);

clg
figure(1)
%plotting alpha and theta, short period
plot(t,y(:,2))
%title('Short Period Homogeneous Response');
grid
axis([0 15 -.2 .2]);
```

64

```
gtext('alpha - rad');
hold on
plot(t,y(:,3));gtext('q - rad/sec');
xlabel('Time, sec'); ylabel('Response Gain');
hold off
pause

figure(2)
%plotting u/U and theta, long period
plot(t,y(:,1))
%title('Long Period Homogeneous Response');
grid
axis;
gtext('u/U');
hold on
plot(t,y(:,4));gtext('theta - rad');
xlabel('Time, sec'); ylabel('Response Gain');
hold off
```

5.   doublet.m

% This program uses EXPM function to find response to pitch doublet

```
clear
dderiv

% Inertial Matrix
in = [Ufps      0      0  0;
       0  Ufps-Zalphadot 0  0;
       0  -1*Malphadot  1  0;
       0      0      0  1];


% Aircraft Matrix
an = [Ufps*Xu   Xalpha   0      -1*g*cos(thetanaut);
      Ufps*Zu   Zalpha  Ufps+Zq -1*g*sin(thetanaut);
      Ufps*Mu   Malpha   Mq          0;
       0      0      1          0];

bn = [ Xde  Zde  Mde  0 ]';

a  = inv(in)*an;
b  = inv(in)*bn;

t1 = 1.0;   % start of doublet, sec
t2 = 2.0;   % midpoint of doublet, sec
t3 = 3.0;   % end of doublet, sec

d0 = -1;              % unit elevat   nput (1 rad) [t.e.u]

tim = 15;             % set end time
t  = 0:0.05:tim;

x = zeros(4,length(t));    % initialize solution matrices
x1 = zeros(4,length(t));
x2 = zeros(4,length(t));
x3 = zeros(4,length(t));

for i = 1:length(t)

  if t(i) >= t1
    de(i)  = d0;
```

```
   x1(:,i) = d0*(expm(a*(t(i)-t1)) - eye(size(a)))*inv(a)*b;
   end

   if t(i) >= t2
    de(i)  = de(i) - 2*d0;
    x2(:,i) = -2*d0*(expm(a*(t(i)-t2)) - eye(size(a)))*inv(a)*b;
   end

   if t(i) >= t3
    de(i)  = de(i) + d0;
    x3(:,i) = d0*(expm(a*(t(i)-t3)) - eye(size(a)))*inv(a)*b;
   end

   x(:,i)  = x1(:,i) + x2(:,i) + x3(:,i);

end

ymin = -2*abs(d0);
ymax =  2*abs(d0);
V = [0  tim   ymin   ymax]';

figure(1)
plot(t,de);grid;axis(V)
xlabel('Time, sec'); ylabel('Elevator, Rad');
%title('Elevator Input')
pause; axis

figure(2)
%plotting alpha and pitch rate
plot(t,x(2,:))
%title('Doublet Response')
grid;gtext('alpha')
hold on
plot(t,x(3,:));gtext('q')
xlabel('Time, sec');ylabel('Response Gain')
hold off
```

6.   sp_bode.m

```
%   This program uses the BODE function to find the
%   short-period response (transfer-function gain and phase)
%   to a harmonic input

clear
dderiv

% Inertial Matrix
in = [Ufps      0       0 0;
       0  Ufps-Zalphadot 0  0;
       0  -1*Malphadot   1  0;
       0      0       0  1];


% Aircraft Matrix
an = [Ufps*Xu   Xalpha   0      -1*g*cos(thetanaut);
      Ufps*Zu   Zalpha  Ufps+Zq -1*g*sin(thetanaut);
      Ufps*Mu   Malpha  Mq            0;
       0      0     1             0];

bn = [ Xde  Zde  Mde  0 ]';

a  = inv(in)*an;
b  = inv(in)*bn;
c  = eye(size(a));
d  = zeros(size(b));

w = logspace(-1,2,150);
[mag,phase,w] = bode(a,b,c,d,1,w);

for i = 1:length(w)
  for j = 1:4
    if phase(i,j) > 0
      phase(i,j) = phase(i,j) - 360;
    end
  end
end

clg
figure(1)
% Plotting alpha and pitch-rate gains
```

```
semilogx(w,mag(:,1));grid;gtext('alpha')
%title('Short-Period Frequency Response')
hold on
semilogx(w,mag(:,2));gtext('q')
xlabel('Frequency, rad/sec');ylabel('Gain')
hold off
pause

figure(2)
% Plotting alpha and pitch-rate phase angles
semilogx(w,phase(:,1));grid;gtext('alpha')
%title('Short-Period Frequency Response')
hold on
semilogx(w,phase(:,2));gtext('q')
xlabel('Frequency, rad/sec');ylabel('Phase, deg')
hold off
```

7.   n_bode.m

```
%   This program uses the BODE function to find
%   the normal-acceleration response
%   (transfer-function gain and phase) to a harmonic input

clear
dderiv

% Inertial Matrix
in  = [Ufps      0       0  0;
        0  Ufps-Zalphadot 0  0;
        0   -1*Malphadot  1  0;
        0       0       0  1];

% Aircraft Matrix
an = [Ufps*Xu   Xalpha   0      -1*g*cos(thetanaut);
      Ufps*Zu   Zalpha  Ufps+Zq -1*g*sin(thetanaut);
      Ufps*Mu   Malpha  Mq            0;
        0        0      1             0];

% Control Matrix
bn = [Xde  Zde  Mde  0]';

a   = inv(in)*an;
b   = inv(in)*bn;
c   = [ Zu  Zalpha  Zq  0 ];
d   = Zde;

w = logspace(-1,2,150);
[mag,phase,w] = bode(a,b,c,d,1,w);

for i = 1:length(w)
  mag(i)   = mag(i)/g*pi/180;          % converting to g's/deg
  if phase(i) > 0
    phase(i) = phase(i) - 360;
  end
end

% Plotting load factor/deg elevator input
figure(1)
semilogx(w,mag);grid
xlabel('Frequency, rad/sec'); ylabel('Normal Acceleration Gain')
```

```
%title('Normal Acceleration Response to Harmonic Input')
pause

% Plotting normal acceleration phase angle
figure(2)
semilogx(w,phase);grid
xlabel('Frequency, rad/sec'); ylabel('Normal Acceleration Phase, deg')
%title('Normal Acceleration Response to Harmonic Input')
```

B. LATERAL-DIRECTIONAL DYNAMICS

1. lat_dir.m

```
% Solves the full 4x4 lateral-directional response
clear
dderiv
!del latdir.dia
diary latdir.dia
in = [Ufps    0      0      0
       0      1      0   -1*Ixz/Ixx
       0      0      1      0
       0   -1*Ixz/Izz  0      1];
an = [YB   Yp  g*cos(thetanaut)   Yr-Ufps
      LB   Lp       0            Lr
      0    1        0            0
      NB   Np       0            Nr];
a = inv(in)*an;
[wn,zeta] = damp(a)
[x,d] = eig(a)
r = [0 0 0 0];

for i = 1:4
  r(i)  = d(i,i);
end

x2 = zeros(4,2);

for j = 1:4
  x2(j,1) = abs(x(j,1));
  x2(j,2) = 180/pi*angle(x(j,1));
end

xx = x2(1,1);
xy = x(3,2);
xz = x(4,3);
x3(:,1) = x2(:,1)/xx;
x3(:,2) = x2(:,2) - x2(1,2);
x3(:,3) = x(:,3)/xy;
x3(:,4) = x(:,4)/xz;
x3

diary off
```

72

2.   rudkick.m

```
%  Response to unit rudder impulse

clear
dderiv

in = [Ufps    0      0      0
       0      1      0   -1*Ixz/Ixx
       0      0      1      0
       0   -1*Ixz/Izz  0      1];

% Plant Matrix
an = [YB    Yp   g*cos(thetanaut)   Yr-Ufps
      LB    Lp        0                Lr
      0     1         0                0
      NB    Np        0                Nr];

% Control Matrix
bn = [Ydr   Yda
      Ldr   Lda
       0     0
      Ndr   Nda];

a = inv(in)*an;
b = inv(in)*an;
c = eye(size(a));
d = zeros(size(b));

t  = 0:.05:10;

[x,y,t] = impulse(a,b,c,d,1,t);

% plotting sideslip (beta) and bank angle (phi)
plot(t,y(:,1));grid;gtext('beta')
hold on
plot(t,y(:,3));gtext('phi')
xlabel('Time, sec');ylabel('Response Gain')
%title('Rudder Kick Response')
hold off
pause

% integrate p for final bank angle
```

```
phi = 0;
t   = 0:.05:100;

[x,y,t] = impulse(a,b,c,d,1,t);

for i = 1:length(t)
    phi = phi + y(i,2)*.05;
end

phi
```

3.   sideslip.m

```
% Solves the full 4x4 lateral-directional response for
% initial sideslip condition

clear
dderiv

in = [Ufps    0    0    0
       0    1    0  -1*Ixz/Ixx
       0    0    1    0
       0  -1*Ixz/Izz  0    1];

an = [YB   Yp  g*cos(thetanaut)   Yr-Ufps
      LB   Lp      0              Lr
       0    1      0               0
      NB   Np      0              Nr];

bn = [ Ydr   Yda
       Ldr   Lda
        0     0
       Ndr   Nda ];

a = inv(in)*an;
b = inv(in)*bn;
c = eye(size(a));
d = zeros(size(b));

t = 0:.05:15;

% calculate sideslip per bank angle

f = [ 0 0 -1*CL ]';
k = [ CnB  Cndr  Cnda
      ClB  Cldr  Clda
      CyB  Cydr  Cyda ];

perphi = inv(k)*f;
betaperphi = perphi(1);

PHI = 10*pi/180;
BETA = betaperphi*PHI;
xin = [ BETA 0 PHI 0 ]'
```

```
[x,y,t] = initial(a,b,c,d,xin,t);

plot(t,y(:,1),'-');grid;gtext('beta')
%title('Dutch Roll Response for Sideslip I. C.s')
hold on
plot(t,y(:,3),'-');gtext('phi')
hold off
xlabel('Time in Seconds')
ylabel('Amplitude')
```

4.   roll.m

```
% Solves the full 4x4 lateral-directional for roll response
% (transfer function gain and phase) due to
% a harmonic aileron input

clear
dderiv

in = [Ufps    0      0      0
        0      1      0   -1*Ixz/Ixx
        0      0      1      0
        0   -1*Ixz/Izz  0      1]

an = [YB    Yp   g*cos(thetanaut)    Yr-Ufps
      LB    Lp        0              Lr
      0     1         0              0
      NB    Np        0              Nr]

bn = [ Ydr   Yda
       Ldr   Lda
        0     0
       Ndr   Nda ]

a = inv(in)*an
b = inv(in)*bn
c = eye(size(a))
d = zeros(size(b))

w = logspace(-1,2,150);
[mag,phase,w] = bode(a,b,c,d,2,w);

for i = 1:length(w)
  for j = 1:4
    if phase(i,j) > 0
        phase(i,j) = phase(i,j) - 360;
    end
  end
end

clg
figure(1)
% Plotting roll angle gain
```

```
semilogx(w,mag(:,3));grid
%title('Harmonic Aileron Input')
xlabel('Frequency, rad/sec');ylabel('Response Gain')
pause

figure(2)
% Plotting roll angle phase
semilogx(w,phase(:,3));grid
%title('Harmonic Aileron Input')
xlabel('Frequency, rad/sec');ylabel('Phase in Degrees')
```

LIST OF REFERENCES

1. Philpott, Tom, "Unmanned 'Toy' Played Big Role in U.S. Targeting of Iraqi Forces," *Navy Times*, March 11, 1991, pp. 8-11.

2. "Gulf War Experience Sparks Review of RPV Priorities," *Aviation Week & Space Technology*, April 22, 1991, pp. 86-87.

3. Shaker, Steven M., Wize, Alan R., *War Without Men: Robots on the Future Battlefield*, Pergamon-Brassey's International Defense Publishers, 1989, p. 6.

4. Rumpf, Richard and Barr, Irwin, "Pioneer is Operationally Capable," *Aerospace America*, February 1989, p. 30.

5. "Pioneer Short Range Remotely Piloted Vehicle Flight Test Based Aerodynamic and Engine Performance," Fleet Combat Systems Laboratory, Pacific Missile Test Center, Point Mugu, California, December 1987.

6. Sandoval, H. R. (ed), "Initial Report for Contractor Development Tests on Baseline Pioneer and Associated Modifications," Unmanned Air Vehicle Office, Pacific Missile Test Center, Point Mugu, California, December, 1988.

7. Lyons, Daniel F., *Aerodynamic Analysis of a U.S. Navy and Marine Corps Unmanned Air Vehicle*, Master's Thesis, Naval Postgraduate School, Monterey, California, June 1989.

8. Tanner, James C., *Development of a Flight Test Methodology for a U.S. Navy Half-Scale Unmanned Air Vehicle*, Master's Thesis, Naval Postgraduate School, Monterey, California, March 1989.

9. Bray, Robert M., *A Wind Tunnel Study of the Pioneer Remotely Piloted Vehicle*, Master's Thesis, Naval Postgraduate School, Monterey, California, June, 1991.

10. Salmons, James D., *Developmental Flight Testing of a Half-Scale Unmanned Air Vehicle*, Master's Thesis, Naval Postgraduate School, Monterey, California, September, 1990.

11. Aitcheson, Kent R., *Stability and Control Flight Testing of a Half Scale PIONEER Remotely Piloted Vehicle*, Master's Thesis, Naval Postgraduate School, Monterey, California, September, 1991.

12. Wilhelm, Kevin T., *Development and Testing of an Unmanned Air Vehicle Telemetry System*, Master's Thesis, Naval Postgraduate School, Monterey, California, September, 1991.

13. Koch, Paul A., *Flight Testing of a Half-Scale Remotely Piloted Vehicle*, Master's Thesis, Naval Postgraduate School, Monterey, California, March, 1992.

14. Graham, Robert G., *Implementation of a Personal Computer Based Parameter Estimation Program*, Engineer's Thesis, Naval Postgraduate School, Monterey, California, March, 1992.

15. Quinn, Patrick J., *An Application of Parameter Estimation to the Stability and Control of the BQM-147 Unmanned Aerial Vehicle*, Master's Thesis, Naval Postgraduate School, Monterey, California, June, 1993.

16. Abbot, Ira H., von Doenhoff, Albert E., *Theory of Wing Sections*, Dover Publications, Inc., New York, 1959, p. 190.

17. Smetana, Frederick O., *Computer Assisted Analysis of Aircraft Performance, Stability and Control*, McGraw-Hill Book Company, New York, 1984.

18. Schmidt, Louis V., *Introduction to Flight Mechanics*, Class Notes, AE-3340, Naval Postgraduate School, Monterey, California, July 1992.

19. Perkins, Courtland D., Hage, Robert E., *Airplane Performance, Stability and Control*, John Wiley and Sons, Inc., New York, 1950, pp. 222-224.

20. Hall, Stan, "Dynamic Modeling", *Sport Aviation*, 30 July 1987, pp. 30-35.

21. Gainer, Thomas G., Hoffman, Sherwood, *Summary of Transformation Equations and Equations of Motion Used in Free Flight and Wind Tunnel Data Reduction Analysys, NASA SP-3070*, 1972.

22. Beer, Ferdinand P., Johnson, Russell E., Jr., *Vector Mechanics for Engineers, Statics*, Fifth Edition, McGraw-Hill Book Company, New York, 1988.

23. Howard, Richard M., *Introduction to Flight Mechanics*, Class Notes, AE-3340, Naval Postgraduate School, Monterey, California, July 1992.

INITIAL DISTRIBUTION LIST

No. Copies

1. Defense Technical Information Center 2
   Cameron Station
   Alexandria, Virginia 22304-6145

2. Library, Code 52 2
   Naval Postgraduate School
   Monterey, California 93943-5002

3. Chairman, Code AA 1
   Department of Aeronautics and Astronautics
   Naval Postgraduate School
   Monterey, California 93943-5000

4. Professor Richard M. Howard, Code AAHo 3
   Department of Aeronautics and Astronautics
   Naval Postgraduate School
   Monterey, California 93943-5100

5. Professor Conrad F. Newberry, Code AANe 1
   Department of Aeronautics and Astronautics
   Naval Postgraduate School
   Monterey, California 93943-5100

6. Mr. Don Meeks, Code AA 1
   Department of Aeronautics and Astronautics
   Naval Postgraduate School
   Monterey, California 93943-5100

7. LT Eric J. Watkiss 1
   2520 Brookline Ct. #112
   Arlington, Texas 76007

8. Mr. Richard J. Foch 1
   Ms. Peggy Toot
   Naval Research Lab, Code 5712
   4555 Overlook Ave. SW
   Washington, DC 20374